TECHNICAL UNIVERSITY DRESDEN
Faculty of Computer Science
Institute for System Architecture

Degree Dissertation

Visualization of Vibrations of Loudspeaker Membranes

Joachim Schlechter

September 30, 2006

Visualization of Vibrations of Loudspeaker Membranes

Degree Dissertation in Media and Computer Science

Faculty of Computer Science
Institute for System Architecture
Technical University Dresden
GER-01062 Dresden
Germany

Printed at LKS Heymann
Dresden, Germany 2006

TECHNISCHE UNIVERSITÄT DRESDEN
Fakultät Informatik
Institut für Systemarchiketur

Diplomarbeit

Visualisierung des Schwingungsverhaltens von Lautprechermembranen

bearbeitet von Joachim Schlechter

Bearbeitungszeitraum:	1. April - 30. September 2006
Betreuung:	Dr.-Ing. habil. Michael Hochmuth, TU Dresden
	Dr.-Ing. habil. Wolfgang Klippel, Klippel GmbH

Visualization of Vibrations of Loudspeaker Membranes
Degree Dissertation in Media and Computer Science
JOACHIM SCHLECHTER
Faculty of Computer Science
Institute for System Architecture
Technical University Dresden

Abstract

The sound reproduction quality of loudspeakers is highly dependable on the vibration and radiation properties of the loudspeaker membrane. With the help of laser measurement techniques the movement of each membrane point can be determined. Hereby a big amount of vibration data is produced which requires an adequate post-processing to supply the loudspeaker engineer with the relevant information about the measured speaker in a quickly perceivable and easily interpretable way.

The task comprises the interpolation of incomplete measurement data, an appropriate data reduction which helps focusing on the important properties of the loudspeaker vibrations and a correction for possible measurement errors. The immediate prediction of the radiated sound pressure enhances the analysis opportunities of the loudspeaker behavior.

In addition to a stroboscopic animation of the vibration pattern a new decomposition technique is presented for the visualization of the measured data. Radial and circumferential modes can be separated and the total vibration can be split into radiating and non-radiating vibration components. This kind of post-processing reveals critical vibration modes, simplifies the interpretation and gives indications for further improvements of the loudspeaker design.

Keywords: Vibration Visualization, Loudspeaker Vibration Analysis, Radiation Modeling, Vibration Decomposition

Contents

Acknowledgements

This project has been made possible in cooperation with Klippel GmbH, a small acoustics company in Dresden, Germany. I am obliged to the team at Klippel GmbH providing me with all needed help to lead this work to a successful result. In particular the fruitful discussions with my supervisor Wolfgang Klippel led always to new ideas and solutions to tricky problems.

I also want to thank my family for the strong support all the time and particularly during the time when I was writing this document. Studying in Dresden would not have been so much fun without my friends and the people of the Students Club P5.

Furthermore I am grateful to Manuela Heinrich for checking my English formulations. Nevertheless I am solely responsible for any remaining misspellings or inappropriate English expressions and I ask in advance for the reader's pardon in these cases.

Joachim Schlechter
September, 2006

Notations

Symbols

a	Acceleration	$[m/s^2]$
c	Speed of sound	$[m/s]$
c_0	Speed of sound in air	$343m/s$ (at 20°)
f	Frequency	$[s^{-1}]$
j	Imaginary number	$j = \sqrt{-1}$
k	Wave number	$k = \omega/c\ [m^{-1}]$, $(k_0 = \omega/c_0)$
p	Sound pressure	$[Pa]$
r	Radius on the cone surface	$[m]$
S	Surface area	$[m^2]$
t	Time	$[s]$
u	Voltage	$[V]$
v	Velocity	$[m/s]$
x	Displacement	$[m]$
Z	Height coordinate	$[m]$
λ	Wavelength	$\lambda = c/f\ [m]$
ω	Angular frequency	$\omega = 2\pi f\ [s^{-1}]$
ϕ	Angle on the cone surface	$[rad]$
ϕ_x, ϕ_v, ϕ_a	Phase angle of x, v, a	$[rad]$
ρ_0	Density in air	$\rho_0 = 1.21kg/m^3$ (at 20°)
σ	Standard deviation	
θ	Angle orthogonal to cone surface	$[rad]$
$H(\omega)$	Complex transfer function	
L_p	Sound pressure level	$L_p = 20\log_{10}\left\lvert\frac{\tilde{p}}{p_{ref}}\right\rvert\ [dB]$
$\vec{r}_i$	Vector to point i on the cone	
$\vec{R}$	Vector to sound modeling point	

Abbreviations

BEM	Boundary Element Method
CAE	Computer Aided Engineering
DA	Distortion Analyzer, made by Klippel GmbH
FEA	Finite Element Analysis
FFT	Fast Fourier Transformation
FPS	Frames Per Second
LDV	Laser Doppler Vibrometry
RGB	Red, Green, Blue color value
RMS	Root Mean Square
SPL	Sound Pressure Level
VB	Visual Basic

AVI	Audio Video Interleaved, movie container format
BMP	Bitmap, picture format
DXF	Drawing Interchange Format
EMF	Enhanced MetaFile, picture format
JPG	Joint Photographic Expert Group, picture format
PNG	Portable Network Graphics, picture format

1 Introduction

1.1 Overview

The development of high-quality loudspeaker systems is a challenging task. The complex interaction of electrical, mechanical and acoustical properties involved in the sound reproduction by loudspeakers is still not perfectly predictable by numerical methods. Therefore measurements of existing speakers remain an essential part of the development process to get a better understanding of the particular properties of the respective loudspeaker leading to an improved design.

Beside measurements of the electric behavior of loudspeakers, the measurement of membrane vibrations delivers valuable information for the optimization of the sound radiation. With the help of modern measurement systems based on laser technology the vibration behavior of each membrane point can be determined over the complete audible frequency range. Hereby a huge amount of data is collected which can become difficult to analyze without an appropriate post-processing.

The post-processing will form the main topic for this work including an adequate visualization of the vibration measurement results. For this the relevant information for a loudspeaker engineer shall be provided by quickly perceivable visual representations. Furthermore helpful tools for analyzing the vibration behavior shall be developed and implemented in an accompanying application software.

The visualization and analysis application has to be adapted to a laser vibration scanning system presently under development at the company Klippel GmbH in Dresden, Germany. This entails a number of restrictions to reach a proper integration into already existing software components while paying attention to the specific characteristics of the scanning process.

The document is structured in the following way. At first a short introduction into the physical basics for loudspeakers and vibration measurements will be given in this chapter. An overview over existing vibration measurement hardware and analysis software will also be included.

The following chapter 2 will present the laser vibration scanner system which acquires the measurement data from vibrating loudspeaker membranes. The properties of the scanning process and the associated control software will provide the basis for the subsequent visualization.

The specification and architecture of the visualization and analysis software is then the content of chapter 3. After having determined the general structure of the software chapter 4 will deal with the detailed implementation. The developed algo-

rithms concerning an interpolation and error correction of the measurement data are described as well as a method for the prediction of the radiated sound pressure. Thereby also a novel decomposition technique will be introduced to provide a powerful tool for a deeper analysis of the vibration behavior. Furthermore the properties of the graphical presentation in the visualization software are presented in an extra section.

In the next chapter the results of the implemented sound pressure modeling are compared with real measurements to evaluate the accuracy of the model. Also the applicability of the developed software is demonstrated conducting an analysis of an example loudspeaker.

Finally a conclusion will be drawn to sum up the results of the work and to discuss the usability of the implemented software. An outlook on future interesting aspects of the vibration visualization and analysis of loudspeakers will complete the work.

1.2 Sound, Vibrations and Loudspeakers

This section is intended to give some theoretical background on acoustics forming the physical base of this work. For those who are not familiar with the working principle of loudspeakers and general acoustical relations, a short introduction shall be given here.

What is Sound?

Sound is the propagation of small pressure disturbances in air. Comparable to the waves appearing if you throw a stone into water sound waves propagate away from a sound source with the speed of sound c which is $343 m/s$ in air at $20°C$. The sound pressure p is often expressed in terms of sound pressure level L_p (also SPL), see (1.1).

$$L_p = 20 \log_{10} \left| \frac{p}{p_{ref}} \right| dB \tag{1.1}$$

That means the sound pressure p is specified in a logarithmic scale which is in accordance with the logarithmic perception of sound by the human ear. The reference sound pressure $p_{ref} = 2 \cdot 10^{-5} Pa$ is the threshold of human sound perception at 1kHz. From this follows that the threshold of perception corresponds to a sound pressure level of $0dB$ while for example during a loud rock concert sound pressure levels around $120dB$ can occur next to the speaker systems.

Some more relations concerning the perception of sound might give a better picture of how the sound pressure level can be understood. About $1dB$ is the smallest notable difference in loudness between two tones while an increase of about $10dB$

is perceived as a doubling in loudness [Zwi 99]. The human ear is able to perceive sound in a frequency range of about $20Hz$ up to $20kHz$ and it has its greatest sensitivity in the mid frequency region (approximately $600Hz$ to $6kHz$) while it is less sensitive to lower and higher frequencies. Regarding this circumstance the sound pressure level L_p is sometimes rated with a standardized A-weighting curve [ISO223] indicated by the unit $dB(A)$ which relates all sound pressure level values to a level of equal loudness at 1kHz.

And what are Vibrations?

A body is called vibrating when it describes an oscillating motion around a rest position. The frequency of an oscillation is defined as the number of complete motion cycles during a period of one second. It is common to express the frequency f of vibrations as angular frequency ω taking regards to the angle of circular rotation during one second, see (1.2).

$$\omega = 2\pi f \tag{1.2}$$

The vibrating motion itself can be characterized by three related physical properties, the displacement x, the velocity v and the acceleration a. Vibrating properties are conveniently expressed as complex measures $\overline{x}$ with a certain vibration amplitude $\widehat{x}$ and a certain phase angle ϕ_x depending on frequency ω, refer to (1.3).

$$\overline{x} = \widehat{x}\, e^{j(\omega t + \phi_x)} \tag{1.3a}$$

$$\overline{v} = \widehat{v}\, e^{j(\omega t + \phi_v)} \tag{1.3b}$$

$$\overline{a} = \widehat{a}\, e^{j(\omega t + \phi_a)} \tag{1.3c}$$

Using this description of complex measures, the relation between displacement x, velocity v and acceleration a can be simply expressed as in (1.4).

$$\overline{v} = \frac{d\overline{a}}{dt} = j\omega\,\overline{a} \tag{1.4a}$$

$$\overline{x} = \frac{d\overline{v}}{dt} = j\omega\,\overline{v} = -\omega^2\,\overline{a} \tag{1.4b}$$

The vibrational behavior is therefore completely described by any of these three measures while the other measures can be deduced by multiplying with the appropriate power of $j\omega$.

Electrodynamic Loudspeakers

A loudspeaker is an electromechanical transducer for converting electrical signals into sound [Ber 54, page 183]. A cross-section of a general loudspeaker is shown in figure 1.1. The conical diaphragm, usually made of paper, is rigidly attached to a

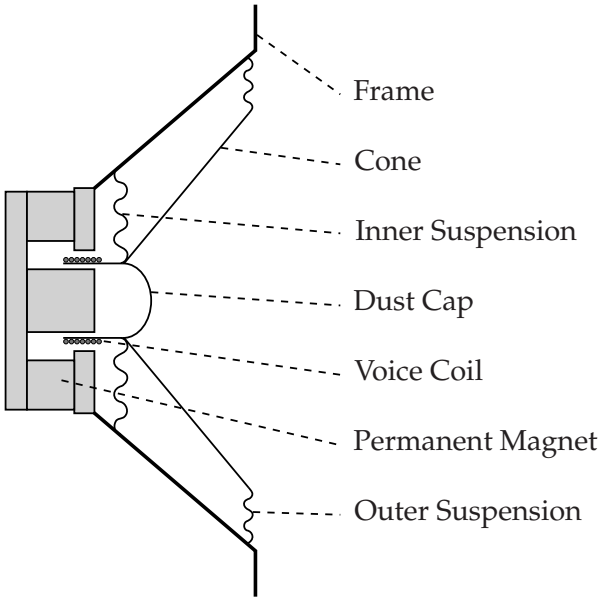

Figure 1.1: Schematic sketch of an electrodynamic loudspeaker.

voice coil. The coil is placed in the radial magnetic field of a permanent magnet and according to Lorentz's law a force is exerted when a signal current is fed through the voice coil. An inner suspension or spider and an outer suspension or rim restrict the movements of the cone to the axial direction. The moving cone surface creates small pressure disturbances in the air in front of the loudspeaker which propagate away as sound waves.

The transformation of the applied electrical voltage u into the finally produced sound pressure p can be divided into two basic steps, see figure 1.2.

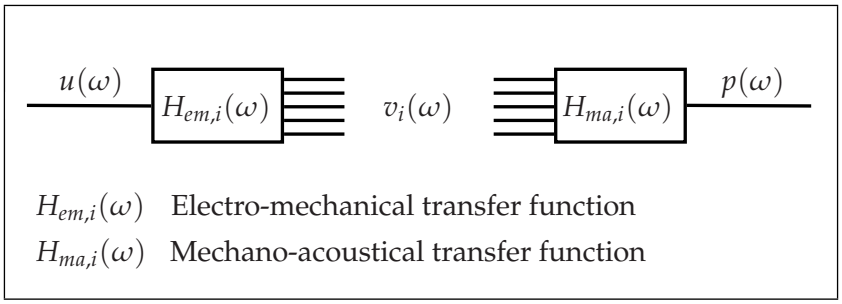

Figure 1.2: Transformation of voltage u into sound pressure p.

The first step describes the electrodynamic transformation from the voltage u into the mechanical movement of the cone, expressed by the velocity v. Since the cone does not necessarily move as a rigid body, rather the velocity v_i at different points i on the loudspeaker membrane shall be considered. The characteristic parameters of this transformation are on the one hand the electrical properties of the voice coil and the magnetic field intensity of the permanent magnet. On the other hand also the mechanical properties of the loudspeaker like stiffness and damping of the suspension and the mass of the moving parts have an influence on this transformation.

The second step is the mechanical-acoustical transformation of the moving cone velocity v_i into the radiated sound pressure p evaluated at a certain listener position. The final sound pressure will be determined by a combination of the radiated sound portion of each membrane point i and the respective distance to the listener point.

The frequency response of a loudspeaker shall be defined as the total produced sound pressure at a certain specified listener position in relation to a constant input voltage u. The frequency response characterizes the loudspeakers influence on the input signal. The ultimate goal of loudspeaker engineering is to realize a prescribed (mostly flat) frequency response in a certain (mostly wide) frequency range [Fra 75]. That means an ideal loudspeaker is supposed to reproduce the input signal without emphasizing or reducing the sound of certain frequency ranges in relation to other frequencies, compare figure 1.3.

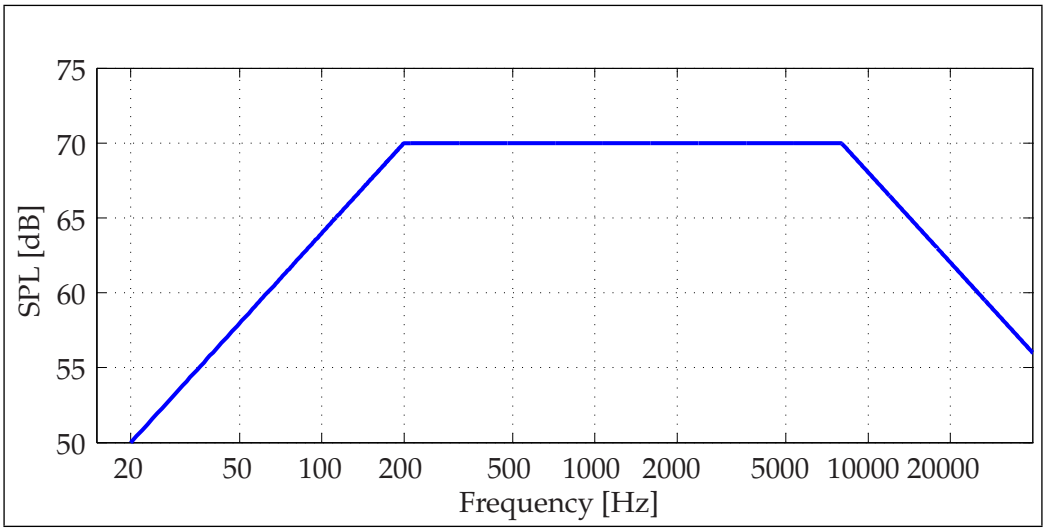

Figure 1.3: Ideal frequency response from 200Hz to 8kHz.

Additionally, the frequency response of the loudspeaker should also be as flat as possible for a mostly broad region of listener points. At very low frequencies loudspeakers usually radiate sound uniformly in all directions, but at higher fre-

quencies they can become quite directive and produce most sound along a straight axis. Often the frequency response is only given on axis at a certain distance in the far-field of the loudspeaker. The far-field of a loudspeaker is characterized by a constant drop of the sound pressure (independent of frequency) with the distance r from the loudspeaker center. It is usually safe to assume far-field conditions in a distance r of three to five times the loudspeaker diameter d.

To reach such a flat frequency response as sketched in figure 1.3 is still a big challenge for loudspeaker designers. Given the extreme difficulty in attempting to cover the whole audible range from 20Hz to 20kHz with a single loudspeaker driver, a high quality speaker system will necessarily consist of several optimized drivers each responsible for a certain frequency range [Col 99, page 9].

The mechanical properties of the loudspeaker have a big influence on the frequency response. The mechanical vibrations depend on the properties of the cone and suspension material, like mass per area, stiffness, damping, and also on the speaker geometry. At low frequencies the cone is usually sufficiently stiff to move as a whole. But above a certain frequency mechanical bending and longitudinal waves appear on the cone (the so-called cone break-up) creating a complex vibration pattern [Fra 75]. If a certain vibration frequency is regarded separately, it is possible to identify more or less distinctive vibration modes which are superposing each other. Each vibration mode is characterized by a certain mode shape which describes the distribution of certain cone regions vibrating in the same direction (in-phase) or in opposite directions (anti-phase). On the cone of circular loudspeakers one can mainly find circumferential and radial modes shapes, compare figure 1.4. A plus sign in the picture means a motion towards the viewer while a minus sign is related to a motion away from the viewer.

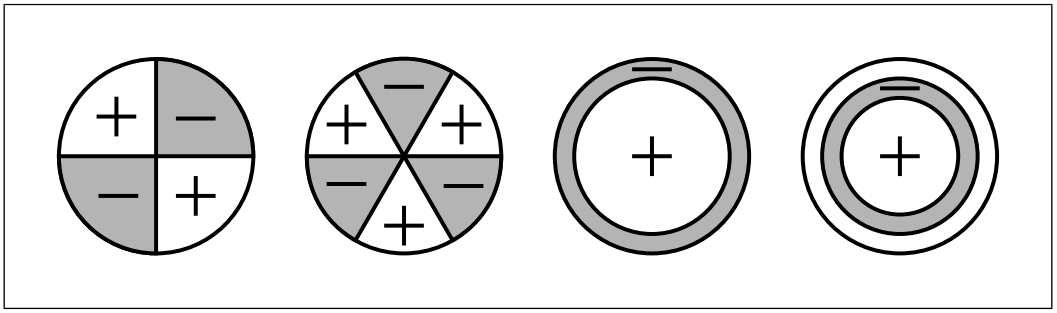

Figure 1.4: The two first circumferential and radial mode shapes.

Provided the cone geometry and all material parameters, a Finite Element Analysis (FEA) can predict the mechanical vibrations by numerical methods. These predictions can coincide with the real loudspeaker behavior only to a certain extent. This is partly because of the difficulty to determine the exact mechanical properties due to inhomogeneous cone materials. A measurement of the real vibrations of a loudspeaker cone can help to evaluate the results of such a FEA model and to fit

the model better to the existing cone properties.

Conducting vibration measurements of the cone can also reveal the reasons of certain problematic dips and peaks in the frequency response. Starting from a better understanding of the vibrational behavior at such a problematic frequency a loudspeaker engineer can find solutions to counteract these dips or peaks and get to a loudspeaker design with a flatter frequency response.

The final sound radiation of the loudspeaker cone depends on the vibration pattern and the cone geometry. Several acoustical models can describe the relation between the velocity of a vibrating surface and the radiated sound pressure. These models differ regarding their accuracy and limitations.

A Boundary Element Model (BEM) can be used to calculate the sound field produced by a vibrating surface with high precision. A disadvantage of BEM modeling is the high computational complexity which leads to a long calculation time for a complete picture of the sound radiation from a single loudspeaker cone.

The point source model describes a much simpler approach to calculate the radiated sound pressure. Making some simplifying assumptions the results of the point source model are less accurate but they can be obtained in much shorter time. In section 4.1.1 the implemented sound radiation model will be discussed in more detail.

1.3 State of the Art

There are several established techniques for measuring vibrations. Some of the most important methods are introduced and compared in this section. Also existing systems and software for post-processing and visualization of the measured vibrations will be reviewed.

1.3.1 Vibration Measurement Techniques

To measure vibrations of a surface point means to determine the displacement, velocity or acceleration of the surface point with a sufficiently high time resolution. The sampling frequency F_s describes the number of taken measurements per second and the highest measurable vibration frequency f_{max} is determined by the Nyquist–Shannon sampling theorem (1.5).

$$F_s >= 2f_{max} \tag{1.5}$$

An upper frequency limit of $f_{max} = 20kHz$ according to the audible range can only be covered with a measurement with a sampling frequency $F_s >= 40kHz$.

The vibrational behavior of a complete surface can be investigated by conducting measurements on many spots on the surface to obtain a dense mesh of vibration data. The spatial resolution of the measurement mesh has to be chosen again in

accordance to the sampling theorem (1.5). But this time not the time difference between two measured samples but the spatial distance between two measurement points has to be considered. A bending wave with a wavelength λ on the cone surface will only be seen in the measurements, if the minimum distance between two adjacent measurement points is shorter than $\lambda/2$. The wavelength of the bending waves is strongly dependent on the cone material. The higher the frequency of the vibration the shorter the wavelength of the bending waves occurring on the cone surface. On a paper cone at a frequency of about $10kHz$ the bending wavelength in radial direction is roughly $1cm$ and therefore a measurement mesh with a resolution higher than about $0.5cm$ would be necessary to see the correct bending motion.

Accelerometer Measurements

Accelerometers are piezoelectric transducers which can be attached to a vibrating body, see figure 1.5. When a piezoelectric material is mechanically stressed, it generates an electrical charge Q across its pole faces which is proportional to the applied force F [BK 82]. Therefore, according to Newton's well known second law of motion $F = m \cdot a$ the measured charge Q is directly proportional to the acceleration.

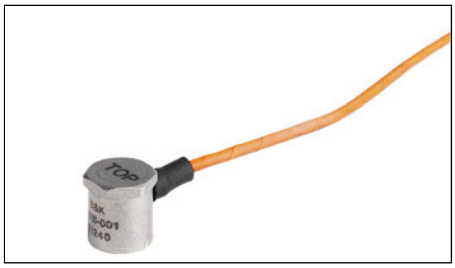

Figure 1.5: Accelerometer, Brüel & Kjær.

Using accelerometers, it is possible to measure vibration with high accuracy as long as the moving body is big and heavy in comparison to the accelerometer. Otherwise the mass of the transducer itself has an influence on the vibration and changes vibration levels and frequencies. Therefore only very small and lightweight accelerometers could be used to measure the vibrations of a loudspeaker diaphragm. But even with the smallest available accelerometers the mass load will considerably change the measured vibrations especially at higher frequencies and on more flexible spots on the membrane. Sufficient accurate measurements can only be made at points next to the connection between voice coil and membrane where the cone is very stiff.

Another difficulty of vibration measurements with accelerometers is the need for a rigid connection between the accelerometer and the measured object. Many techniques of mounting accelerometers onto vibrating devices like threaded studs, magnets or glue are hardly advisable to use for loudspeaker membranes. A pos-

sible mounting method is the use of a thin layer of bees-wax for sticking the accelerometer on the cone [BK 82]. Considering the problems of measuring the vibrations of loudspeaker membranes with accelerometers non-contact measurement techniques seems favorable.

Laser Doppler Vibrometry

The Laser Doppler Vibrometry (LVD) works on the basis of optical interference [Pol 03]. The laser beam with an optical wavelength λ_L (HeNe-lasers: $\lambda_L = 632nm$) strikes a point on the vibrating object and is reflected back to a photo detector. Due to the Doppler effect a frequency shift f_D occurs in the back scattered beam which is proportional to the normal velocity v on the surface, (1.6).

$$f_D = 2v/\lambda_L \tag{1.6}$$

This frequency shift can be detected with the help of laser interferometry, see figure 1.6. In the interferometer the laser beam is split into a measurement beam

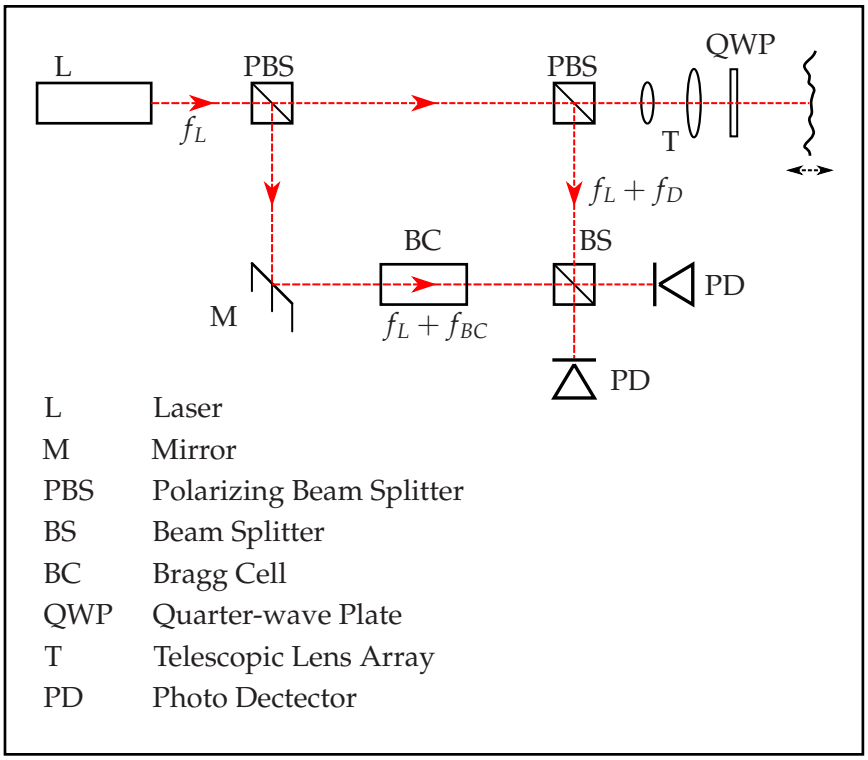

Figure 1.6: Schematic optical arrangement of a heterodyne interferometer of Mach-Zehnder type [Joh 05].

and a reference beam using a polarizing beam splitter [Joh 05]. A quarter-wave plate rotates the polarization of the backscattered light by 90° and another beam

splitter guides it to the detector where both beams are combined again. The two photo detectors are used to receive twice the signal power.

The vibration of the object leads to a Doppler phase shift $\phi_D(t)$ in the measurement beam due to a varying beam length which is proportional to the objects surface displacement $x(t)$, (1.7).

$$\phi_D(t) = 4\pi x(t)/\lambda_L \tag{1.7}$$

In the common heterodyne interferometer type as shown in figure 1.6, the reference laser beam is additionally shifted in frequency by an acousto-optic modulator (Bragg cell). The most common shift frequencies f_{BC} are $40MHz$ and $70MHz$.

Given the light intensities of the reference I_r and measurement beam I_m, the total intensity I_{tot} at the photo detector follows relation (1.8), compare [Gås 02, page 55].

$$I_{tot} = I_r + I_m + 2\sqrt{I_r I_m}cos(2\pi(f_{BC}t - \phi_D(t))) \tag{1.8}$$

By phase demodulation of the measured light intensity signal the displacement $x(t)$ can be obtained. Without the introduced frequency shift ($f_{BC} = 0$) it would not be possible to distinguish the direction of the vibration because of the symmetric cosine function. Applying modern digital demodulation techniques it is possible to get a very accurate displacement signal with a resolution below $1pm$ [Joh 05].

Laser Doppler Vibrometry is an excellent vibration measurement technique. A disadvantage is only the high price of today's commercial available LDV scanning systems. The expensive optical components and data acquisition hardware as well as the market dominating position of few LDV system producers lead to prices in the range of above 50,000$. For the application of measuring loudspeaker membranes the opportunities and accuracy of LDV seems a bit excessive. Therefore a different laser vibration measurement technique is applied in the vibration measurement system developed at Klippel GmbH. The applied triangulation laser technique will be presented in chapter 2 and is supposed to reach a much lower cost of the total vibration system.

1.3.2 Post-Processing Software

A powerful software for visualization and analysis of measured vibration data is an important tool for the investigation of vibration related problems. There are general measurement analysis programs like MATLAB® and its free counterpart Scilab as well as specialized software packages dedicated to certain measurement devices. A standardized file format for data exchange between different analysis programs does not exist, but commonly an import and export of different measurement files is possible for instance using ASCI files with the pure measurement data or the popular MATLAB file format.

MATLAB and Scilab

MATLAB is a high-level technical computing language and interactive environment for algorithm development, data visualization, data analysis, and numeric computation [Mat 04]. MATLAB is essentially a programming environment optimized for extensive mathematical computations with big matrices and complex numbers. Its computing language allows to perform arbitrary mathematical operations and to display the results in the desired way.

Scilab was developed at INRIA (Institute National de Recherche en Informatique et Automatique), France, as a free numerical software package. The open source software project is maintained by the Scilab Consortium, `www.scilab.org`. Both, MATLAB and Scilab are similar regarding their usage and calculation power. While the former focuses more on professional applications and contains better possibilities of presenting results, Scilab is more common for educational tasks.

Any data analysis can be done with the help of either MATLAB or Scilab, but both need to be programmed first. That means an engineer using these tools needs to develop the analysis scripts which shall conduct the desired post-processing. The approach is perfect for research and development applications as well as for educational purposes. However, in a specific production environment a dedicated software specifically designed for the analysis of a certain type of measurements can provide a more comfortable interface and also allows the software operation by users without deeper programming knowledge.

Polytec Scan Viewer

Almost all producers of vibration measurement devices also offer suitable software solutions for visualization and analysis of the measurement results. Polytec, one of the main producers of LDV devices, provides aside its main measurement software package (PSV Software 8.3) a free viewer for the measurement data, figure 1.7.

With the scan viewer you can investigate 2D or 3D scans of Polytec laser measurements [Pol 06]. Many possibilities of displaying the measured vibrations are offered, generally as geometrical offset and coloration of the basic geometry of the measured object. This technique will also be used in the software application developed within the scope of this work, see section 4.2.1 for details.

The broad visualization capabilities of the Polytec Scan Viewer apply for arbitrary scanned surfaces and are therefore hardly adapted to special scanning objects like loudspeaker cones. The multitude of supplied information is rather complex and the essential contribution of the vibrations to the final sound radiation might not be evident. Interesting vibration analysis methods like investigation of the radiated sound or mechanical vibration modes are not included in the viewer, but referred to external software packages.

Certainly, the main application of the vibration measurement system by Poly-

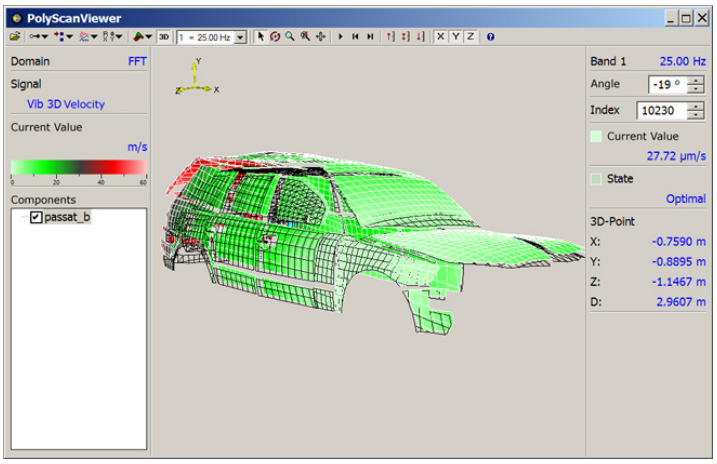

Figure 1.7: Polytec Scan Viewer 1.1 Screen Shot.

tec for automotive and aerospace development determines the relevance of certain analysis methods. In this area the common intention behind measurements on vibrating objects is the characterization of vibrational sources in order to keep their negative influences as small as possible. Of main interest are the insulation of vibrations and investigations of stress and stability connected to high vibration levels. The sound radiation of surfaces is mainly interesting when a vibrating device produces too much noise. In these cases commonly known sound and vibration reduction solutions can be applied until the total produced noise has decreased below a certain given limit.

The vibration measurement of loudspeaker cones serves a different intention, namely the optimization of the radiated sound in terms of a prescribed frequency response. Beside the influence of the electronic components, the geometry and material properties of the cone and the suspension are mainly responsible for the radiated sound. Therefore a detailed analysis of both, vibration and sound radiation properties is necessary to detect and understand problematic peaks and dips in the frequency response with the goal to further improve the speaker design.

To face these demands on an optimized measurement system the Klippel company is developing a new device for measuring vibrations of loudspeaker cones. An accordingly optimized visualization and analysis software will be developed in the frame of this work paying attention to the special requirements dealing with loudspeaker cones.

2 The Vibration Measurement System

In this chapter the existing vibration measurement system is briefly described. Delivering the measured vibration data it is the starting point for the actual task of this work: the visualization of the measurement data. The vibration measurement system has been developed at Klippel GmbH Dresden and is still in a continuing improvement process.

2.1 Triangulation Laser Measurement Technique

Due to the lightweight and elastic cone material only a non-contact vibration measurement technique can be used for scanning the vibrations all over the cone area. Instead of the Laser Doppler Vibrometry, as introduced in section 1.3.1, the vibration measurement system developed at Klippel GmbH is based on a triangulation laser. This type of laser is usually applied for distance measurements but can also be applied to measure vibrations. In figure 2.1 the working principle of a triangulation sensor is shown.

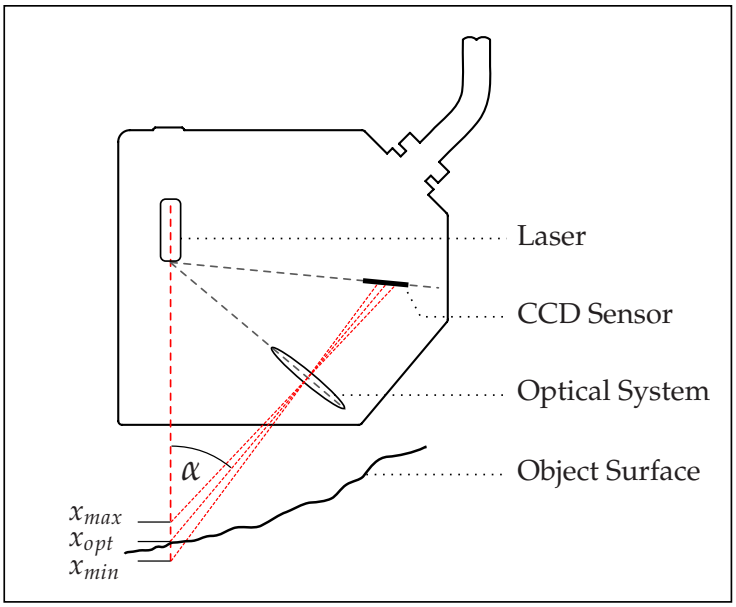

Figure 2.1: Laser triangulation distance sensor, Keyence LK-G32.

A laser beam is diffusely reflected by the measurement surface and mapped by

an optical lens system on a CCD detector (charge-coupled device) as used in digital cameras, [Koh 98, page 48]. A displacement x of the surface leads to a shift of the focal point on the CCD sensor and the surface displacement can be derived from the position of maximal light intensity on the CCD.

The triangulation laser has as certain working distance from x_{min} to x_{max} as indicated in figure 2.1. Outside of this working range the reflected laser beam is not focused on the CCD. For the applied triangulation laser the following specifications in table 2.1 are important for the vibration measurement [Key 05].

Model	Keyence LK-G32 sensor head
Reference distance d_{ref}	$30mm$
Measuring range $[x_{min} - x_{max}]$	$\pm 5mm$, for $F_s = 50kHz$: $x_{min} = -1.8mm$ to $x_{max} = 5mm$
Resolution Δx	$0.05\mu m$
Linearity	$\pm 0.05\%$
Sampling Frequency F_s	$1kHz, 2kHz, 5kHz, 10kHz, 20kHz, 50kHz$

Table 2.1: Specification of the triangulation laser sensor.

According to the sampling theorem (1.5) a sampling frequency $F_s >= 40kHz$ is necessary to measure vibrations in the audible frequency range up to $f_{max} = 20kHz$. Using the $F_s = 50kHz$ mode of the Keyence laser sensor fulfills this requirement.

A disadvantage of the triangulation principle is the relatively short reference distance of $d_{ref} = 30mm$. It has to be assured that the cone is never touched by the sensor head, because the cone as well as the sensor could then be damaged [Poh 06]. Furthermore the vibration measurement would give wrong results if the cone hit the enclosure of the laser sensor. Therefore an intelligent sensor positioning is necessary while scanning a cone surface. Knowing the geometry of already scanned surface points can help to decide whether it is safe to move the laser sensor closer towards the cone.

It can happen that the sensor can not be optimally adjusted at certain geometries (e.g. steep slopes, narrow gaps) on the target surface. Then the vibration data can not be collected at these points and an interpolation method has to be used to derive geometry and vibration data from adjacent points, see section 4.1.1 for further details.

2.2 Mechanical Scanning System

The voice coil is restricted to movements in only one direction (Z dimension). Thus the measurement of the displacement in this direction is sufficient in loudspeaker applications. One displacement sensor is used to scan 2 dimensions (radius r and angle ϕ) of the cone surface. The mechanical setup can be realized by using three

step motors, an electronic control system and a robust mechanical frame as illustrated in figure 2.2.

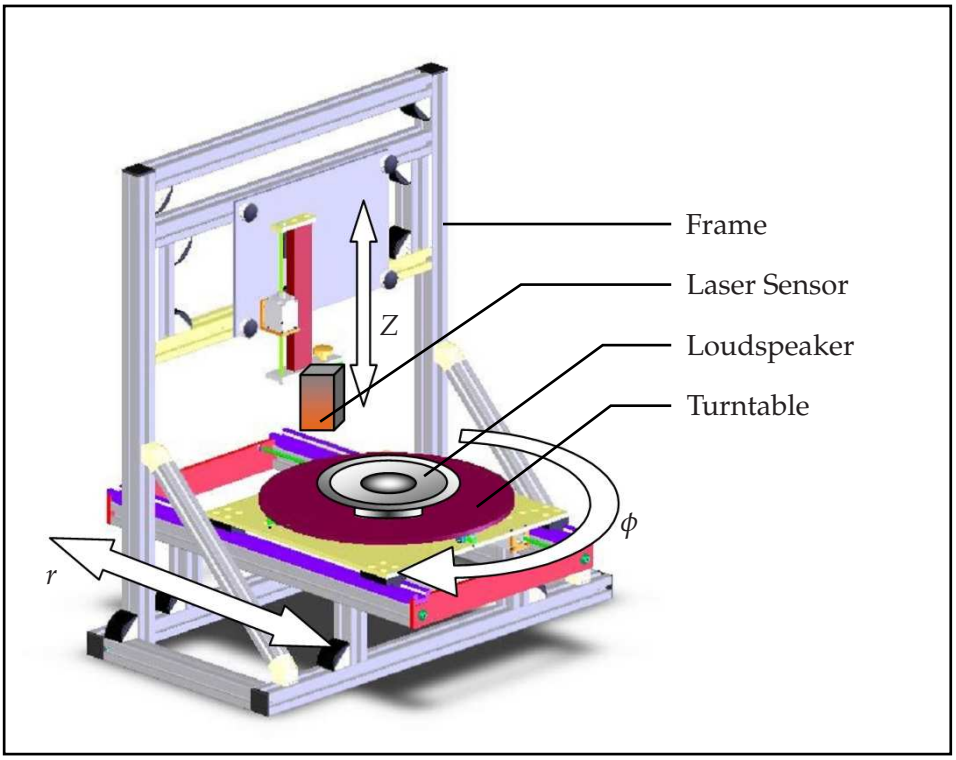

Figure 2.2: Loudspeaker vibration measurement system.

In addition to the components shown in figure 2.2 a motor box control device is responsible for the movements of the laser sensor and the turntable, and a signal acquisition device measures the vibration signals. Instead of moving the laser sensor the loudspeaker under test is rotated by a turntable (ϕ coordinate) and shifted by a linear actuator (r coordinate). An additional step motor is required to adjust the laser to the optimal distance $d = x_{opt}$ in the Z dimension.

To assure a safe movement of the laser sensor over the surface, at first all points on one radius r are scanned before proceeding to the next radius. It is possible to start the scanning in the center of the cone as well as on a point on the outer radius, see figure 2.3.

2.3 Acquisition of Vibration Data

The triangulation laser can measure the displacement of a surface as described in section 2.1. To measure the vibration at one measurement point a certain input voltage signal $u(t)$ has to be applied to the loudspeaker and the respective displacement signal $x(t)$ is measured by the laser sensor. The voltage signal has to in-

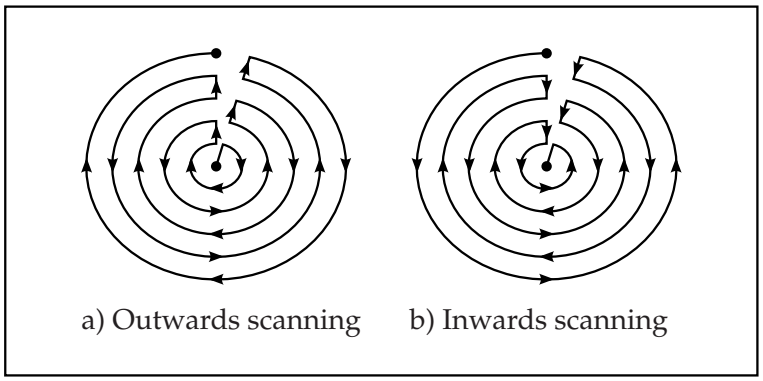

Figure 2.3: Alternative scan paths on the target surface [Poh 06].

clude all frequencies where the vibration of the loudspeaker shall be investigated. This can be accomplished by a sinusoidal frequency sweep starting from the lower frequency limit f_{min} and rising logarithmically to the upper frequency limit f_{max}.

A constant amplitude of the input voltage at all frequency would lead to very low displacements at higher frequencies, because the displacement x of the loudspeaker cone is approximately proportional to $1/f^2$ above the resonance frequency f_0. Thus a sinusoidal sweep with constant voltage generates $x_{peak}(f_0) = 1mm$ at the resonance frequency $f_0 = 20Hz$ but would produce only $x_{peak} = 1nm$ peak displacement at $20kHz$ (compare the resolution of the laser sensor $\Delta x = 50nm$).

An inversely shaped amplitude of the input voltage u can be used to compensate the decay of the displacement at higher frequencies and provide a sufficiently high resolution and signal-to-noise ration (SNR). For example figure 2.4(a) shows a sinusoidal sweep signal where the instantaneous frequency varies logarithmically from $100Hz$ to $10kHz$. The amplitude is not constant but rises quadratically with frequency from $0.1mV$ up to $10V$rms.

The frequency spectrum of the stimulus $U(\omega)$ is presented in figure 2.4(b). The sweep time of about $100ms$ produces distinct frequency components at a distance of about $10Hz$ giving sufficient resolution at higher frequencies. The amplitude profile and the logarithmic sweep speed result in a shaping of the frequency components rising proportional to f^2 which leads to a approximately constant displacement level.

Since the shaping is not relevant for further analysis it is more convenient to calculate the transfer function $H_x(\omega)$ by referring the displacement $X(\omega)$ to the voltage $U(\omega)$ of the stimulus, (2.1).

$$H_x(\omega) = \frac{X(\omega)}{U(\omega)} \tag{2.1}$$

The transfer function $H_x(\omega)$ now shows the displacement relative to a constant input voltage of $1V$.

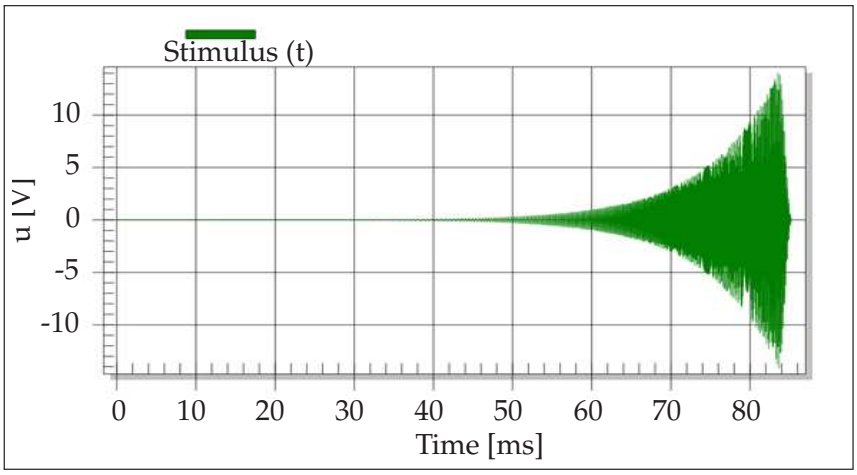

(a) Stimulus time signal.

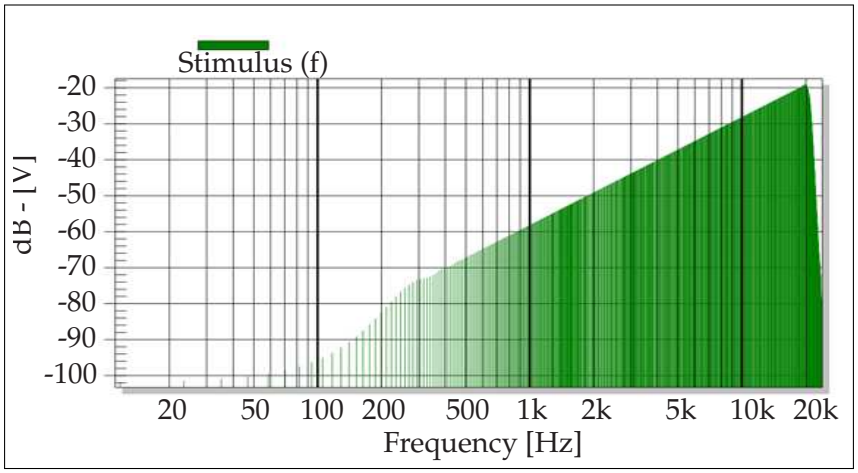

(b) Stimulus frequency content.

Figure 2.4: Input voltage signal for displacement measurement.

Repeating the measurements with the same stimulus 2^n times and averaging the measured displacement responses will improve the signal to noise ratio by $3 \cdot ndB$. Since a single sweep is relatively short extensive averaging (e.g. 128 times) can be applied improving the SNR by more than $20dB$. In this way a sufficiently accurate displacement transfer function can be acquired at each measurement point.

A complete scan of a loudspeaker cone will take quite a long scanning time because only about 4 to 5 specified points can be measured per minute. A sufficiently accurate loudspeaker scan will consist of ca. 1000 - 2000 measurement points depending on the size of the cone and the frequency range of interest. Therefore a robust control software is necessary which allows the scanning process to be run without special supervision e.g. over night.

2.4 Control of the Scanning Process

The scanning process can be controlled by the *3D Scanning Software* running on a PC. The software has been developed using Visual Basic 6.0 during an internship at Klippel GmbH [Poh 06] and it is capable of conducting scans of a complete loudspeaker cone and save the results in a file.

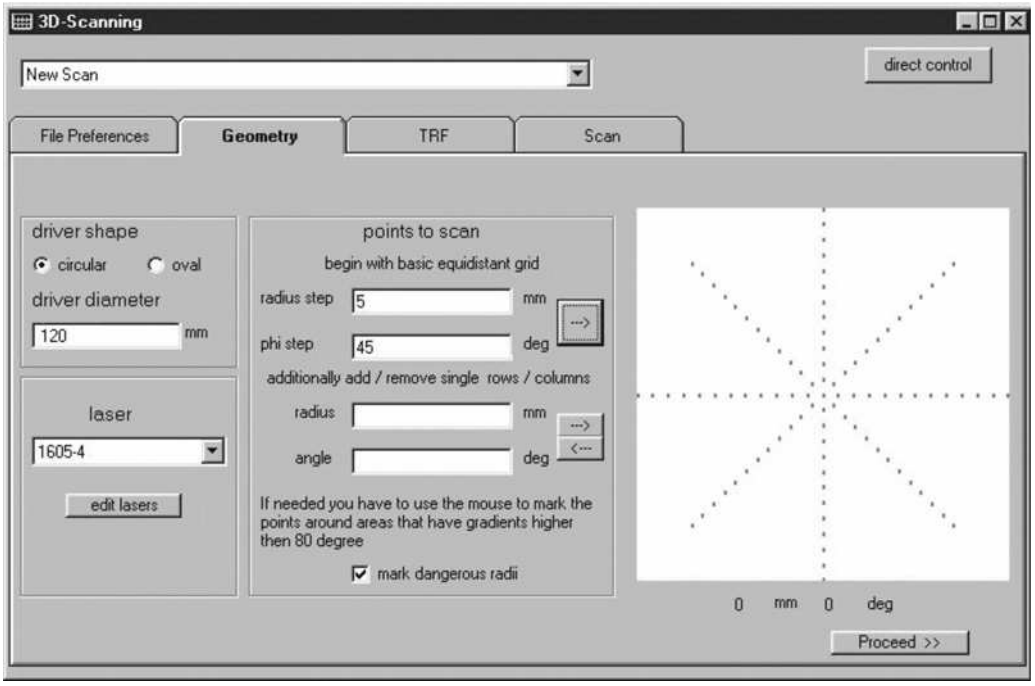

Figure 2.5: Setup of the measurement grid [Poh 06].

Key elements of the scanning software are:

- Setting up the scanning parameters and displaying the scan progress.
- Controlling the positioning of the laser sensor via the motor box.
- Controlling the measurement of the displacement transfer function via the data acquisition hardware.
- Project and file management.

Setting up the Scanning Parameters

It is possible to precisely define a grid of measurement points which shall be included in the scan. According to the positioning of the sensor and the turntable the measurement grid is defined by the coordinates r and ϕ, compare figure 2.5. The user can choose an equidistant scanning grid, but also additional radii or angles

can be inserted or removed. This can be useful, if a certain subarea of the cone locally requires a higher spatial scan resolution. The possible non-uniformness of the scanning grid has implications on the interpolation methods, see section 4.1.1.

A separate dialog is related to the setup of the transfer function measurement. The user can specify a subset of points from the measurement grid, where the transfer function shall be determined. For the remaining points only the geometry of the cone will be measured. The detailed settings of the transfer function measurement, like the frequency range, the input signal shaping and the number of averages per point can be chosen in an additional setup dialog.

When all scanning parameters are defined the scanning process can be started. Now the laser sensor will automatically approach all marked points and conduct transfer function measurements where this is specified.

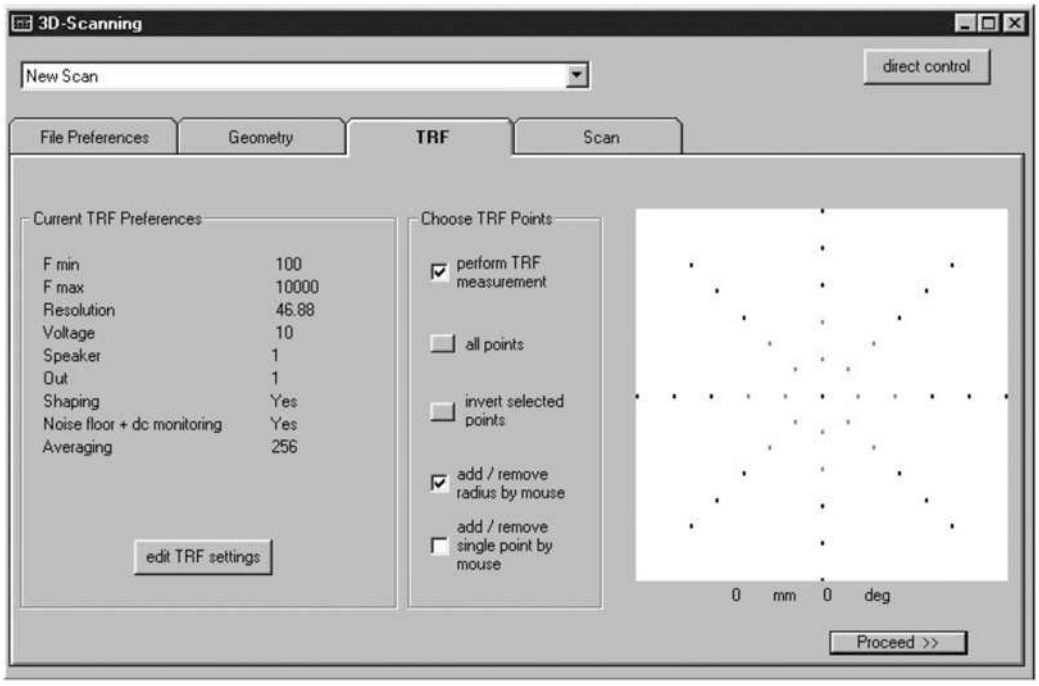

Figure 2.6: Setup of the transfer function measurement [Poh 06].

Controlling the Position of the Laser Sensor

The *3D Scanning Software* can control the positioning of the laser sensor with the help of the motor control box. This is accomplished by an ActiveX control encapsulating the communication with the micro controller inside the motor control box and the PC via USB.

Three step motors are responsible for the positioning of the laser sensor over the cone surface. One motor controls the height Z of the laser sensor, one motor can

rotate the turntable and change the angle ϕ and one motor moves the complete turntable back and forth and adjusts like this the measured radius r, compare figure 2.2.

It is possible to send movement commands to the motor control and to receive status information. The movement commands include the number of steps, the direction and the respective motor which should conduct this movement. Status information contain for example the state of stop position sensors indicating the end of the movable range for each motor, the state of step counters for each motor and also the quality of the laser signal.

Each time the laser scanning system is started a calibration routine is necessary to initialize all three motors to a known position. During the scanning process each point of the measurement grid is approached and the height Z is adjusted to the optimal working distance of the triangulation sensor.

An underground check routine is necessary to avoid contact between the sensor head and the loudspeaker. If the laser sensor can not be adjusted optimally then the respective measurement point is marked as not measured and the scan proceeds with the next point. This can lead to gaps in the measurement grid which have to be filled up by appropriate interpolation, see 4.1.1.

Transfer Function Measurement

When the laser sensor has arrived at a point designated for a transfer function measurement the data acquisition device can start the data collecting. The used acquisition device is the Klippel Distortion Analyzer (DA), a hardware platform developed at Klippel GmbH including a high performance digital signal processor and a two-channel 24bit AD/DA converter [Kli 03].

The USB communication between the scanning software and the DA is managed again by an ActiveX interface component. All setup data is sent to the DA and the results are received each time the measurement of one point is finished.

The measurement itself is conducted as described in 2.3 playing a sinusoidal sweep and measuring input voltage u and the displace signal x. After a transformation of the signals into frequency domain by doing a Fast Fourier Transformation (FFT) the transfer function $H(\omega)$ can be calculated according to (2.1). The procedure is repeated accordingly to the specified number of averages and the averaged transfer function is sent back to the scanning software.

During the scanning the actual progress and an estimation for the remaining time is displayed in the scanning software. It is possible to interrupt the scanning process and proceed or refine older scans as long as the position of the loudspeaker on the turntable is not changed.

Project and File Management

All data belonging to one loudspeaker measurement are combined to a scan project. The chosen project settings are saved in a separate text-based initialization file. In this was it is possible to load an older scan project and continue an interrupted scan process or define additional measurement points to increase the grid resolution.

A binary status file contains information about the measured geometry of the cone and status information for each point of the measurement grid. The status flags contain for example information whether a point is designated for a transfer function measurement and whether it was successfully measured.

Finally the results of the transfer function measurements are saved in a third file which can be imported in Scilab, refer to section 1.3.2. The transfer function for each point is saved in a separate matrix consisting of three columns, first the measured frequency, second the amplitude of the transfer function in [dB] and third the phase of the transfer function.

Further files of the scanning software which are relevant for the planned visualization software are a global system initialization file and a file containing localized text messages. The system initialization file includes a few globally relevant properties like the language of the application and a list of the recently opened project files.

The language file is used for the localization of the strings in message boxes and error messages. This ensures an application of the software in multi-lingual environments.

3 The Visualization Software

The main contribution of this work is the development and implementation of a visualization system for the analysis of the measured data. The focus lies on finding optimal data representations which bring out the relevant information, simplify the interpretation and give indications for further improvements of the loudspeaker design.

An appropriate animation shall intuitively illustrate amplitude and phase relation of the membrane vibration. Also the contribution of each membrane point to the total radiated sound pressure has to be determined and illustrated. Possible errors and noise in the measurement data shall be recognized and suppressed by appropriate measures. Furthermore a virtual increase of the measurement resolution by non-linear interpolation can realize a sufficient visualization quality even for a small number of measurement points.

3.1 Specification and Requested Features

The application of the visualization software is well defined. A loudspeaker shall be checked thoroughly for possible flaws in vibration behavior and sound reproduction. For this, the surface of the loudspeaker was scanned with the laser scanner device described in chapter 2 and now the measurement data are going to be analyzed.

In cooperation with Klippel GmbH some basic requirements for the visualization software were defined which consider the integration into the existing software.

Basic requirements

- Adaption to existing software environment
- Accuracy of all calculations and figures
- Sufficient animation performance
- Intuitive user interface
- Multi-language support

During the development process the final functionality and user interface became more and more clear and resulted in a list of features which should be included in the visualization software.

Tasks:

- Interpolation of the measurement data.
- Suppression of errors and noise.
- Calculation of the total radiated sound pressure level depending on the listener position.
- Data reduction with the intention of focusing on relevant information.
- Visualization and animation of the surface motion and phase relation at all frequencies.
- Broad data export possibilities.

The realizations of these tasks can be found in the respective sections in chapter 4. A detailed monitoring of the implementation progress concerning the tasks and additional subtasks was a helpful feedback. Through this the actual implementation state of all planned software features could be compared with the time schedule and a possible delay in the software development would have been quickly recognized.

3.2 Architecture of the Application

The choice in software architecture for the visualization software was confined by a number of restrictions. Firstly the scanner and the visualization software are intended to be merged into one single application in future. As the existing scanner application was developed using Microsoft Visual Basic 6 (VB) the choice of a different programming language would have complicated an integration of both modules to an intolerable extent.

A disadvantage of the usage of Visual Basic is the restriction to Microsoft operating systems. But on the other hand the simple user interface design process allows a quick software development and the focusing on the implementation of functional algorithms without much overhead.

Visual Basic is neither optimal for the implementation of extensive mathematical operations nor for the creation of interactive 3D animations as needed in the visualization application. This can be compensated by the comfortable integration of external ActiveX components which can better deal with these tasks, compare figure 3.1.

The KlModuleMat (or simply Mat module) is an ActiveX component developed at Klippel GmbH which realizes a direct interface between Visual Basic and Scilab adding by this the mathematical opportunities of Scilab to VB applications, consult section 1.3.2 for a description of Scilab.

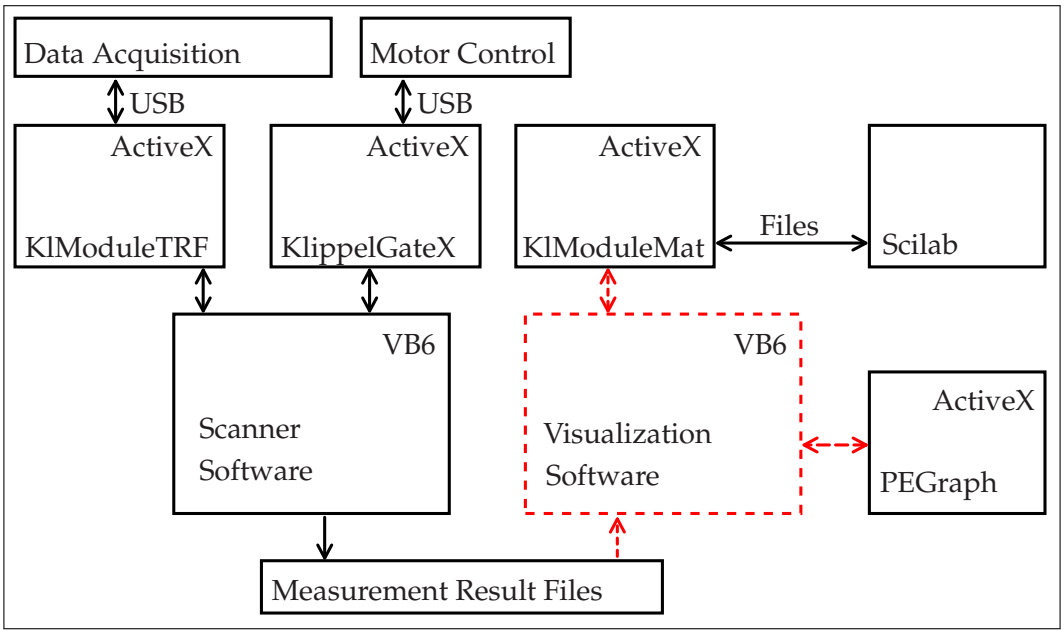

Figure 3.1: Integration of the visualization application into existing software components.

Likewise, the graphical capabilities of VB can be extended by the ActiveX components of ProEssentials (PEGraph6) by Gigasoft. The PEGraph package comprises a set of graphical controls supporting the quick creation of 2D and 3D scientific diagrams including realtime animation.

The current implementation of the visualization software is capable of reading the project files created by the scanner software while in future both applications will be integrated into one program and then also a direct transfer of the measurement results to the visualization will be possible.

The Mat Module

The Mat module component establishes an asynchronous data transfer between Visual Basic and Scilab as mathematical scripting environment. Using this interface it is possible to pass arbitrary input values or arrays together with a respective operation script for execution to Scilab.

When the execution of a Scilab script is started by the Mat module, temporary files are created where the input parameters are saved in a form that is readable for Scilab. Then the respective script is executed and a specified set of result values is returned back to Visual Basic. During the script execution the VB application has to wait until the Mat module throws an event which indicates the finishing of the calculations. In case an error occurred during the script execution, the VB application has access to the output text produced by Scilab which can help to

debug the script.

A big advantage of the transfer of mathematical functionality to Scilab is the high performance especially while conducting extensive operations on big matrices including complex numbers. The algorithms in section 4.1 would take much longer time if they had to be implemented directly in VB.

Another advantage is the interchangeability of the Scilab script without recompiling or even restarting the VB application. That means for the software development process it is possible to do changes in the Scilab script and see the results directly in the VB application. Furthermore, the functionality of the single scripts, e.g. the interpolation routine or the sound pressure modeling routine, are exchangeable in the Scilab script as long as the specification of input and result parameters is not affected. Because of the independent working of the Scilab scripts it is also possible to develop and debug the scripts without starting the visualization software.

A current disadvantage of the interaction between VB and Scilab using the Mat module is the performance loss due to the inefficient data transfer using temporary files. There are plans to refactor the interface to achieve a quicker data transfer.

PEGraph Components

ProEssentials PEGraph from Gigasoft is a commercially distributed set of Visual Basic components which offer the capabilities of creating scientific graphic objects by simple interfaces. These graphic objects allow an extensive customization of their appearances and in the latest version PEGraph 6, there are also 3D objects included which can be changed and displayed in real-time.

One of the first tasks concerning the development of the visualization software was the evaluation of the possibilities of PEGraph 6 regarding its applicability for a real-time 3D animation of a vibrating loudspeaker cone. A simple 3D loudspeaker was created and animated using the 3D-object from PEGraph. Performance tests running on a modern laptop showed a smooth animation of the loudspeaker cone with a frame rate above 25 frames per second (FPS) and an object size up to a number of about 2500 vertices, see figure 3.2.

The animation contained both a continuous updating of the geometry of the cone and the colors of the faces. A number of 2500 vertices was regarded as sufficient for the application of the PEGraph in the visualization software. A disadvantage is that each face of the 3D object has only one fixed color and does not support some kind of color interpolation in between the vertices. Therefore a relatively dense graphical mesh is needed to achieve a smooth color transition.

It is possible to change the meshing method to increase the graphical resolution while maintaining the number of vertices. Instead of using a rectangular mesh which is deformed to represent a circular cone shape it is possible to create a completely new mesh based on triangles, see figure 3.3.

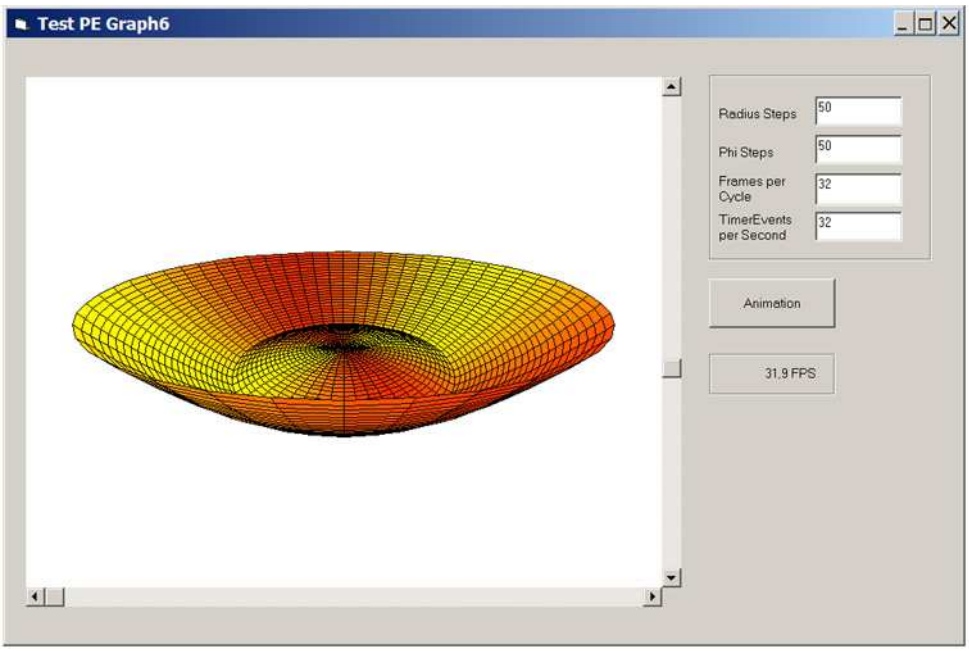

Figure 3.2: Test of the graphical capabilities of PEGraph 6.

The advantage of the triangular mesh would be a nearly constant spatial resolution all over the cone and a much higher number of faces while consisting of the same number of vertices. The regular spatial resolution would improve the visual quality and also the accuracy of the vibrational behavior, because the highest visible wavelength on the cone depends on the spatial resolution, compare section 1.3.1 on page 7.

The rectangular mesh with a constant number of radial and angular divisions has a spatial resolution which is dependent on the radial position. The faces on the outer region of the cone have a smaller circumferential resolution than the faces in the center. This is fortunately less critical for the vibration analysis of a circular loudspeaker cone, because circumferential vibrations are of less importance in comparison to radial vibrations.

The implemented visualization solution is finally based on a rectangular mesh due to practical reasons. First the laser scanner can easily follow radial and angular paths by involving only one step motor while the triangular mesh would require a more sophisticated scanning scheme. Also the data handling becomes much easier in a rectangular pattern represented by simple arrays and would be more complicated with a varying number of points per radius. Finally all analysis algorithms are based on rectangular arrays and their performance is based upon quick matrix operations in Scilab which would not been applicable in the same way for the triangular mesh. Especially the data interpolation and the noise reduction, see section 4.1, would become much more difficult to implement and most prob-

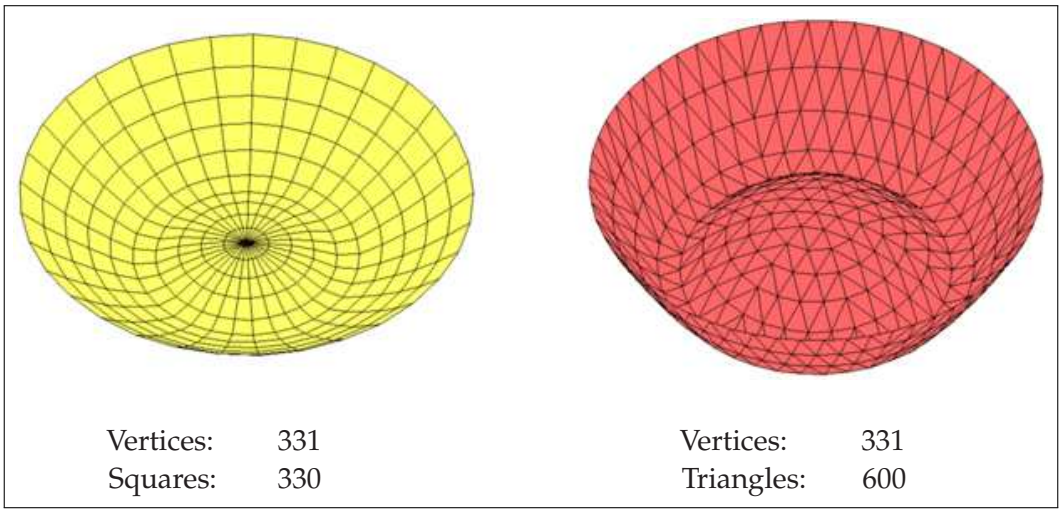

Figure 3.3: Two variants of meshing a circular loudspeaker cone.

ably slower. Nevertheless a triangular surface remeshing remains an interesting alternative to the implemented rectangular mesh.

4 Implementation

Based on the decisions concerning the specification and general architecture of the visualization software in this chapter a detailed description of the main implementation issues will follow.

The software is structurally and functionally divided into the mathematical operations in Scilab and the user interface and graphical representations in Visual Basic. Following this separation section 4.1 will address the algorithms and calculations implemented in Scilab and subsequently in section 4.2 the integration of the calculations into the VB application will be described.

4.1 Algorithms and Calculations

4.1.1 Interpolation of Measurement Data

The data collected during one loudspeaker measurement can be represented by one big data structure which is called Z-matrix. Saved in a file by the scanner application this data structure will be read in by the visualization application.

The Z-matrix contains a regular grid of measurement points along the r and ϕ dimension of the cone surface, see figure 4.1. For each point it includes the measured geometry (Z dimension), amplitude and phase of the measured displacement transfer function and a set of flags which are important for the scanning procedure.

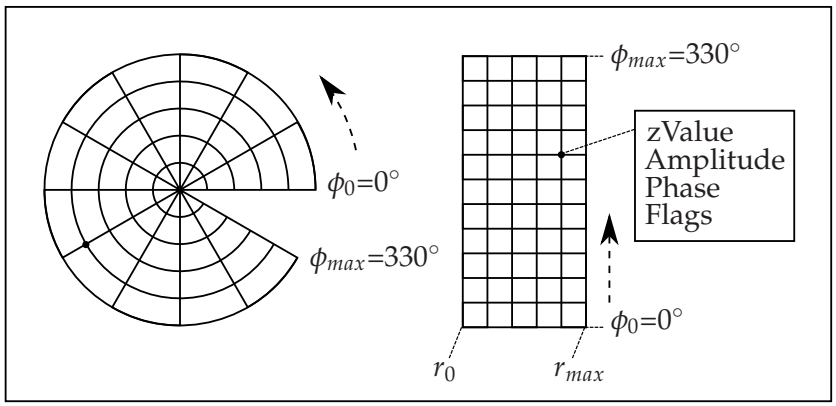

Figure 4.1: Measurement grid and respective data structure.

Due to the characteristics of the scanning process it can happen that certain

points or regions in the Z-matrix are missing information about the geometry or the transfer function data.

This can have different reasons, for instance the scanning process might have been interrupted before all points were scanned. Then the missing points contain a flag which indicates that the measurement has not yet taken place. Another reason could be, that certain points were not selected for transfer function measurement in the scan setup to speed up the scanning. At these points the geometry information is available but the vibration data is missing. Finally a third possibility is the failing of the laser scanning due to a too steep slope in geometry so the laser sensor could not be adjusted optimally without touching the cone surface. At these points neither geometry information nor vibration data could be determined.

Interpolation within the Measurement Grid

The first task for the implementation algorithm will be to fill up the missing geometry and vibration data in the measurement grid. This is necessary to get a connected 3D cone surface for the visualization, see figure 4.2.

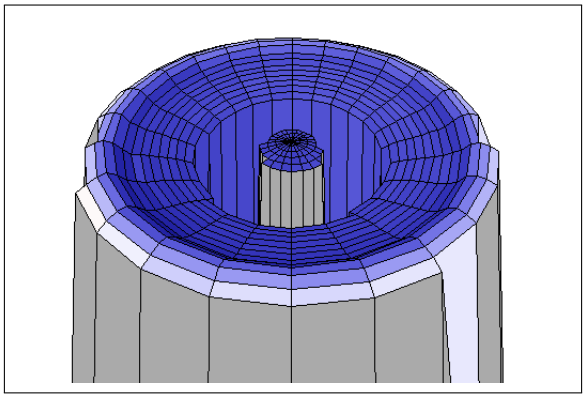

Figure 4.2: Visualization of an example loudspeaker without interpolation.

On the example loudspeaker cone in figure 4.2 there are two broader regions where the geometry and vibration data is missing. One region is a nearly circular ring near the center of the cone while the other region lies at the outer edge of the cone.

The missing points can be interpolated in radial direction, in circumferential direction or by a 2-dimensional approach. In each case the missing points would be filled up by a weighted measure derived from existing measurement points in close neighborhood of the missing gap.

Two special properties of the measurement grid increase the difficulty for an interpolation method. First the grid is not really rectangular but in fact it is a ring. That means the grid points at an angle ϕ_{max} will be connected back to the points at the first angle ϕ_0 and furthermore the single faces are not rectangular but their

inner edge is shorter than the outer edge, see figure 4.1.

The second difficulty relates to the fact that the grid in not necessarily equally spaced with constant steps in radial and angular direction. It is possible to define an arbitrary distribution of intermediate radial and angular grid lines by manually inserting or removing single grid lines in the scan setup.

Facing the difficulties above no standardized surface interpolation algorithm could be applied. Thinkable would have been a 2D spline interpolation or a weighting filter function comparable to the smoothing method which will be introduced in the following section.

Instead, an adapted interpolation algorithm was developed considering the special properties of loudspeaker cone meshes. The interpolation is divided into two steps. In the first step all partly incomplete cone radii are filled up by a linear interpolation between the two existing measurement points adjacent to the missing gap, see figure 4.3.

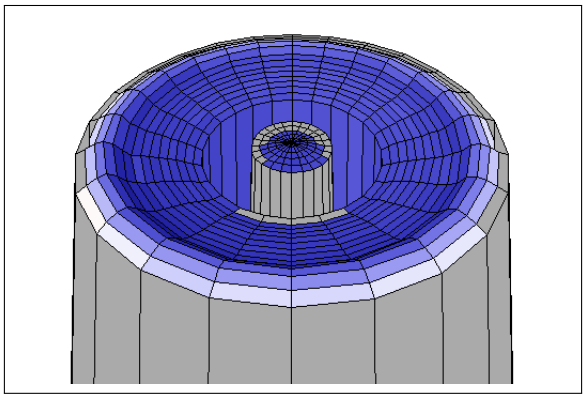

Figure 4.3: Interpolation of incomplete radii.

The interpolation is continued over a complete circle if necessary as long as at least one point exists along the respective radius. Like that the continuity of the cone surface over all angles is assured.

The rotational symmetry of a circular loudspeaker cone supports the idea of interpolating first in circumferential direction. This does not apply perfectly for arbitrarily shaped loudspeakers, but in these cases a subsequent smoothing of the interpolated data will level out unintended steps in the surface geometry. The smoothing will also decrease the linearity of the interpolation and therefore it provides a helpful tool to optimize the interpolation and to remove errors at the same time, refer to section 4.1.2.

The interpolated points are illustrated in a neutral gray color to indicate the extent of the unmeasured areas. On the other hand the measured points are colored here related to the vibrational amplitude, refer to section 4.2.1 for the different coloration schemes.

In a second interpolation step all remaining regions are filled up. Now only

complete missing circumferential grid lines can be left and the interpolation works along each angular grid line, compare figure 4.4.

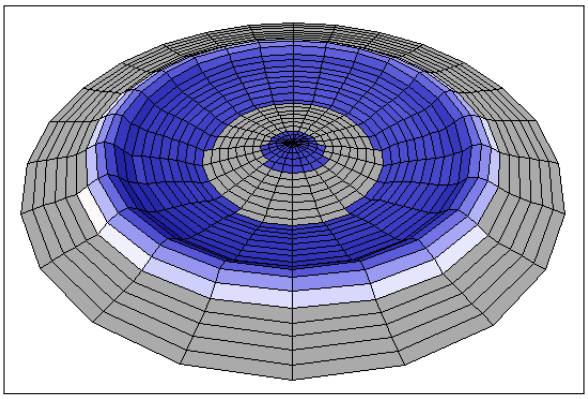

Figure 4.4: Second interpolation step along the angular grid lines.

Where a missing gap is surrounded by existing points, again a linear interpolation can be applied between the adjacent points. Otherwise, missing points at the outer or inner edge are filled up by constant continuation of the geometry of the respective edge.

Linear Interpolation of Geometry and Vibration Data

At each interpolated measurement point four properties have to be treated in a proper way, the z height of the geometry, the amplitude and phase of the displacement transfer function and the flags containing meta information about the respective point.

The missing z geometry values can be linearly interpolated by a straight line between the adjacent existing points with height z_{start} and z_{end}, refer to figure 4.5 for an example interpolation along an angular grid line.

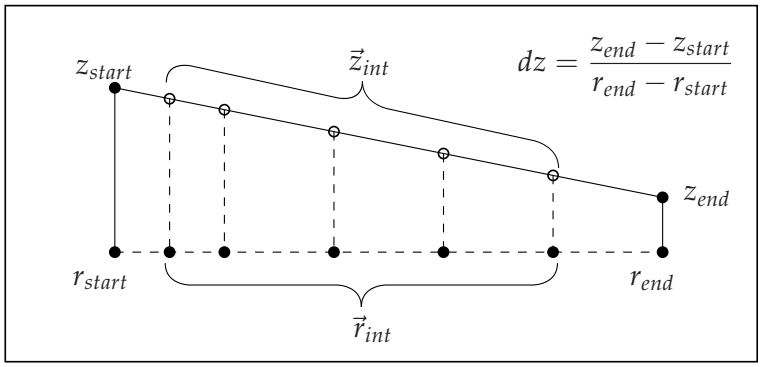

Figure 4.5: Linear interpolation of height z.

The interpolation of a vector $\vec{z}_{int}$ of irregularly spaced points in between can be done by first determining the slope dz of the line (4.1).

$$dz = \frac{z_{end} - z_{start}}{r_{end} - r_{start}} \tag{4.1}$$

Then the missing $\vec{z}_{int}$ values can be linearly filled up by (4.2)

$$\vec{z}_{int} = z_{start} + dz \cdot (\vec{r}_{int} - r_{start}) \tag{4.2}$$

The displacement transfer function H_x is given by an amplitude $\widehat{a}_x$ and a phase angle ϕ_x for each measured frequency (4.3).

$$H_x = \widehat{a}_x \cdot e^{j\phi_x} \tag{4.3}$$

The interpolation is intended to fill up the vibration image at one certain frequency f. Therefore only one amplitude and phase value at each measurement point is of interest.

As the displacement transfer function amplitudes $\widehat{A}_x$ are provided by the scanner application in the unit [dB mm/V] they have to first be converted into non-logarithmic values (4.4).

$$\widehat{a}_x = \frac{1}{1000} \cdot 10^{\left(\frac{\widehat{A}_x}{20}\right)} \quad [\mathrm{m/V}] \tag{4.4}$$

The interpolation of complex numbers, like the displacement transfer function, is mathematically not uniquely defined. To determine the missing vibration data two variants seem appropriate, see figure 4.6.

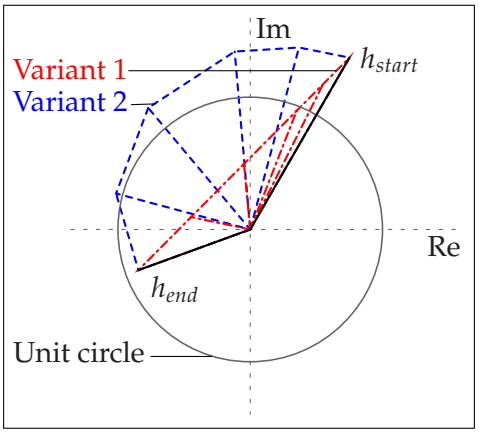

Figure 4.6: Two variants of interpolating between complex numbers.

The first variant describes a linear interpolation between h_{start} and h_{end} within the complex number plane. This line can be achieved by a separate linear interpolation

of the real parts and the imaginary parts of h_{start} and h_{end}. The resulting vibration will be a linear transition between both adjacent vibrating points.

For the second variant a different approach is chosen. Here the amplitude and the phase of h_{start} and h_{end} are interpolated separately. This type of interpolation describes a spiral in the complex number plane, compare figure 4.6. The advantage of this interpolation scheme is a better reconstruction of the actual surface motion. Mechanical bending waves on the cone surface will exhibit a nearly constant amplitude but different phase angles at different positions on the surface. The second interpolation type will maintain this constant amplitude while the first interpolation type will lead to an uneven amplitude distribution.

Therefore the second variant was implemented in the interpolation algorithm used in the visualization software. The missing amplitudes $\widehat{a}_x$ can be linearly interpolated like the z values in (4.2). The only difference is now that completely missing areas at the outer cone region will not be continued with constant vibration amplitude. They will rather be stopped from vibrating by setting the amplitude there to zero to give a clearer picture of the actually measured region in the center.

The interpolation of phase angles ϕ_x is more tricky because the interpolation between the start angle ϕ_{start} and the final angle ϕ_{end} has to be done along the unit circle of complex numbers, see figure 4.7. For this the involved phase angles have to be converted into complex vectors and rotated around the unit circle in the correct ratio.

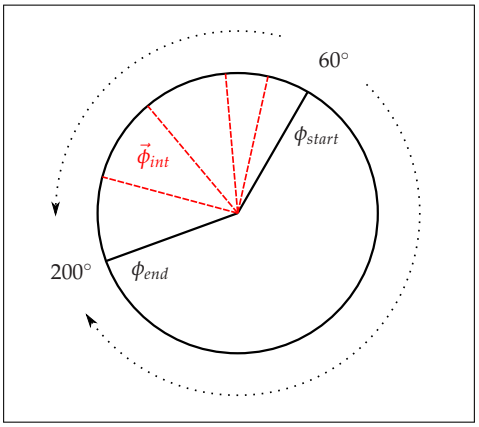

Figure 4.7: Phase interpolation along the unit circle.

A problem is constituted by the two possible interpolation ways, clockwise or counterclockwise around the circle. As long as the Nyquist sampling criterion for the maximal distance of the two adjacent measurement points is fulfilled, refer to (1.5) in section 1.3.1, then the correct interpolation way would always be the shorter one. If the sampling criterion is fulfilled then the angular difference between the phases of two adjacent points has to be smaller than 180°.

The phase interpolation has been implemented in the following way (4.5).

$$\vec{\alpha} = \frac{\vec{r}_{int} - r_{start}}{r_{end} - r_{start}} \tag{4.5a}$$

$$\vec{\phi}_{int} = \arg\left\{ e^{j\phi_{start}} \cdot \left(\frac{e^{j\phi_{end}}}{e^{j\phi_{start}}} \right)^{\vec{\alpha}} \right\} \tag{4.5b}$$

Like this it is assured that the interpolated phase angles will follow the shorter way on the unit circle.

If the sampling criterion is not fulfilled, then it can happen that the interpolated phase angles behave in a strange way. It might occur that independently interpolated adjacent gaps in the measurement grid will not be interpolated in the same direction and especially during the animation of these wrongly interpolated points clearly visible artifacts will be produced in the vibrational motion. These phase errors at interpolated points occur more probably at higher vibration frequencies where the wavelengths of the respective bending waves on the cone surface are shorter.

The problem is less distinct due to the neutral gray coloration of the interpolated points which emphasizes the unreliable character of the vibration data at these points. Nevertheless only by a dense enough measurement grid it can be assured that no phase interpolation errors will occur.

Interpolation to increase the visual Resolution

In addition to the previous interpolation of missing points in the measurement grid it is also possible to apply an interpolation of additional values to increase the resolution of the cone surface for a better visual representation. Complete additional grid lines in radial and angular direction can be included in the visualization grid to reach a smoother surface representation.

For the automatic insertion of additional grid lines it is necessary to describe the final mesh resolution by an appropriate parameter. It seems a useful approach to define a certain maximum number of points in the final grid and then the interpolation algorithm can use this contingent to fill up the existing grid in order to reach an optimal visual representation.

The radial mesh structure does not produce mesh faces with equally long sides, as the length of the circumferential face edges is always dependent on the actual radius. The length s of a circular segment above a certain angle α is defined as (4.6).

$$s = 2r \sin\left(\frac{\alpha}{2}\right) \tag{4.6}$$

Assuming a regular division of the radius r_{max} into r_{step} equal parts and another regular division of the complete circle of 360° into ϕ_{step} equal parts it is possible to find a relation between r_{step} and ϕ_{step} where the outer ring of the cone surface

consists of nearly quadratic faces. Provided s is set equal to r_{max}/r_{step} then equation (4.6) can be transformed into (4.7).

$$\begin{aligned} \frac{r_{max}}{r_{step}} &= 2r_{max}\sin\left(\frac{\alpha}{2}\right) \\ \frac{r_{max}}{r_{step}} &= 2r_{max}\sin\left(\frac{\pi}{\phi_{step}}\right) \\ \frac{1}{r_{step}} &= 2\sin\left(\frac{\pi}{\phi_{step}}\right) \end{aligned} \tag{4.7}$$

For higher numbers of $\phi_{step} >= 5$ then (4.7) can be approximated by (4.8).

$$\begin{aligned} \frac{1}{r_{step}} &\approx \frac{2\pi}{\phi_{step}} \\ \frac{\phi_{step}}{r_{step}} &\approx 2\pi \end{aligned} \tag{4.8}$$

That means to get approximately quadratic mesh faces at the outermost ring there have to be about 6 times as many angular subdivisions as radial subdivisions. But then all inner mesh faces will be squeezed in angular direction. Starting from (4.8) it seems more appropriate to get approximately quadratic faces at a distance of $r_{max}/2$ from the center. Then all faces outside of half the maximal radius will be stretched and all faces inside will be squeezed. This leads to a relation of 3 times as many angular subdivisions as radial ones which means $\phi_{step} = 3 \cdot r_{step}$.

That relation served as starting point to share additional subdividing lines. Due to the symmetry of loudspeakers it seemed a reasonable approach to insert only additional angular subdivisions when a symmetric distribution can be maintained. The remaining contingent of additional points are at first regularly inserted as new radial subdivisions and if there were still points left to form complete radial grid lines, the mesh was further refined starting at the outer edge where the faces are larger due to the lower angular resolution, compare figures 4.8 a) to f).

Circular regions which entirely consist of not measured values are not further refined because the vibration values there are not exact anyway. It seems more appropriate to use the contingent of additional visualization points in regions which were actually measured, compare figure 4.8 c).

The insertion of additional grid lines is done using the same interpolation principles as before while filling up the missing gaps. The only difference is that now the interpolated points should not be colored gray but rather show the right meta-data according to the status of the surrounding points. That is accomplished by copying the meta-data from each of the two existing points as appropriate to half of the interpolated points in between.

The problem of possibly inconsistent phase interpolation as mentioned before becomes now even more serious because incorrect interpolated points might not

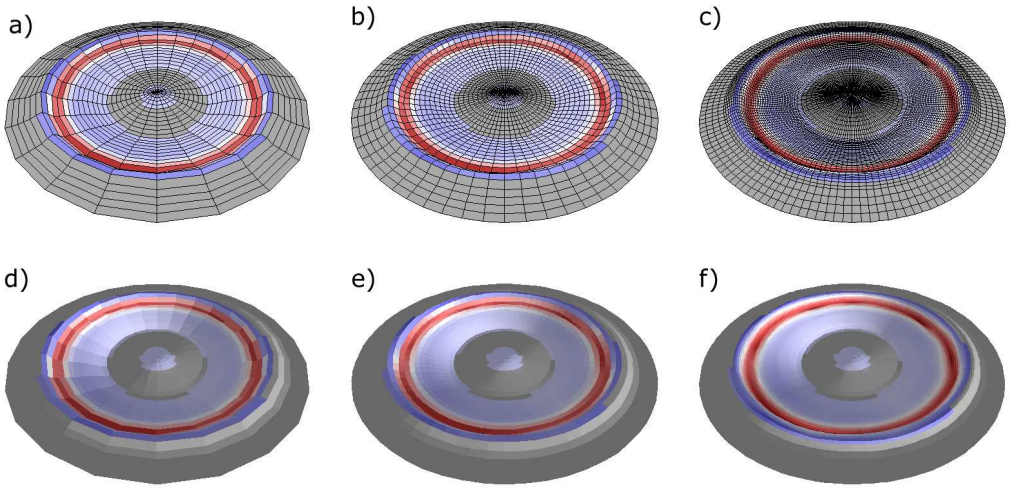

Figure 4.8: a) Measurement grid (744 points), b) Interpolated (2000 points), c) Interpolated (10000 points), d) - f) Shaded versions of the pictures above.

be immediately recognized as invalid. In figure 4.9 b) an example of inconsistent interpolation due to a too low measurement resolution is shown.

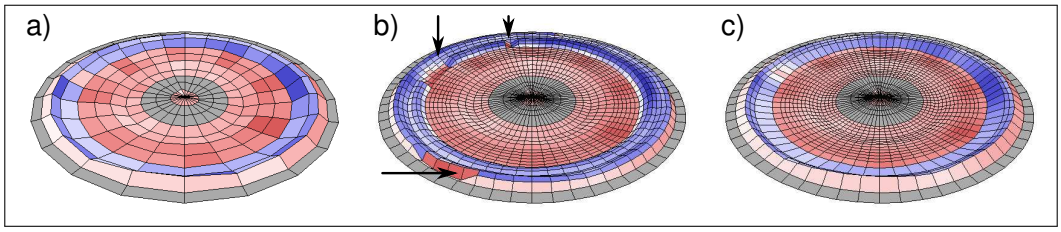

Figure 4.9: a) Original measurement grid (288 points), b) Incorrect phases (2000 points), c) Omit dangerous regions (2000 points).

The original grid resolution in figure 4.9 a) has been refined to a number of 2000 points and artifacts are clearly visible. These artifacts are especially distracting the user while watching an animation of the vibration.

To face this problem it is necessary to recognize the cases where an incorrect phase interpolation might occur. A good indication is a violation of the Nyquist theorem. If there are adjacent points vibrating with nearly opposite phases, then there is a high probability that a phase interpolation error will occur.

Two methods can now be applied to securely avoid an incorrect interpolation. A first and easy measure is to omit the interpolation if there is a danger of interpolating wrongly. By this the additionally available interpolation points can be used to refine the remaining grid further, see figure 4.9 c).

A second method can be to fall back to the first variant of interpolating between complex numbers as illustrated in figure 4.6 on page 33. Interpolating along a

straight line through the complex number plane avoids the indeterminism of two possible ways around the unit circle. But this kind of interpolation would have exactly the same visual effect as omitting the interpolation because now the interpolated points always produce a straight line between the two existing adjacent vibrating points.

4.1.2 Error Correction and Smoothing

The vibration data provided by the triangulation laser sensor can contain measurement noise, for example due to imperfectly reflecting surfaces or too low vibrational amplitude. This measurement noise can be filtered out of the final picture to increase the clarity of the illustration. Small-scale random noise can be effectively removed by applying a 2D Gaussian filtering, compare figure 4.10.

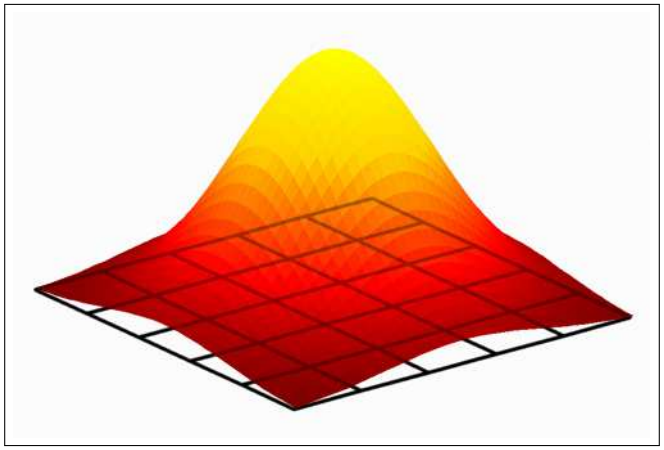

Figure 4.10: 2D Gaussian smoothing filter [Hof 06]

.

The Gaussian filtering is commonly used in picture processing to blur the effects of high-frequent noise and artifacts. The same technique can be applied to arbitrary data in a 2-dimensional mesh, e.g. the geometry and vibration data on the cone surface. The one-dimensional Gaussian distribution has the form (4.9).

$$g(x) = \frac{1}{\sqrt{2\pi}\sigma} \cdot e^{-\frac{x^2}{2\sigma^2}} \tag{4.9}$$

where σ is the standard deviation of the distribution.

The actual smoothing is achieved by convolution of the measurement data with a discretized Gaussian distribution. By this the data value of each measurement point is weighted with the Gaussian function including the values of surrounding measurement points. The order of the smoothing describes the number of surrounding data values which are included in the smoothing process. The one-

dimensional discretized filter function $g_2(x)$ of second order with $\sigma = 0.6$ can be seen in figure 4.11.

$$g_2(x) = \frac{1}{1000} \cdot \begin{array}{|c|c|c|c|c|} \hline 3 & 165 & 664 & 165 & 3 \\ \hline \end{array}$$

Figure 4.11: Gaussian filter function of second order.

The filter matrix $G_2(x, y)$ for smoothing two-dimensional data structures can be found by vectorial multiplication of $g_2(x)$ with its transposed form $g_2^T(x)$, see figure 4.12.

$$G_2 = \frac{1}{1000} \cdot \begin{array}{|c|c|c|c|c|} \hline 0 & 0 & 2 & 0 & 0 \\ \hline 0 & 27 & 110 & 27 & 0 \\ \hline 2 & 110 & 441 & 110 & 2 \\ \hline 0 & 27 & 110 & 27 & 0 \\ \hline 0 & 0 & 2 & 0 & 0 \\ \hline \end{array}$$

Figure 4.12: Gaussian filter matrix of second order.

The standard deviation σ should be chosen in a way that the values at the borders of the filter matrix are sufficiently small. A value of about $\sigma = 0.3$ times the filter order leads to good results.

Due to the symmetry of the Gaussian function it is possible to separately conduct a filtering in x-direction and in y-direction instead of conducting a complete two-dimensional filtering which speeds up the calculation time.

The Gaussian smoothing can be applied at different stages of the complete interpolation process and also separately for the geometry, amplitude and phase of the vibration. It does not seem profitable to interpolate the z geometry because the distance measurement of the triangulation laser is very accurate. But at interpolated points a smoothing of the geometry can help to improve the visual quality and to cover the linear interpolation.

Special care has to be taken at the borders of the mesh to assure a correct behavior of the smoothing filter. In circumferential direction the continuity of the surface can be assured by filtering an overlapping mesh. The n adjacent angular grid lines have to be circularly continued at both sides of the mesh while using a Gaussian filter of order n. In radial direction the outermost line of points should also be

copied n times to conserve the energy in the smoothed vibration. See figure 4.13 for an example what a correct mesh should look like before applying the Gaussian smoothing.

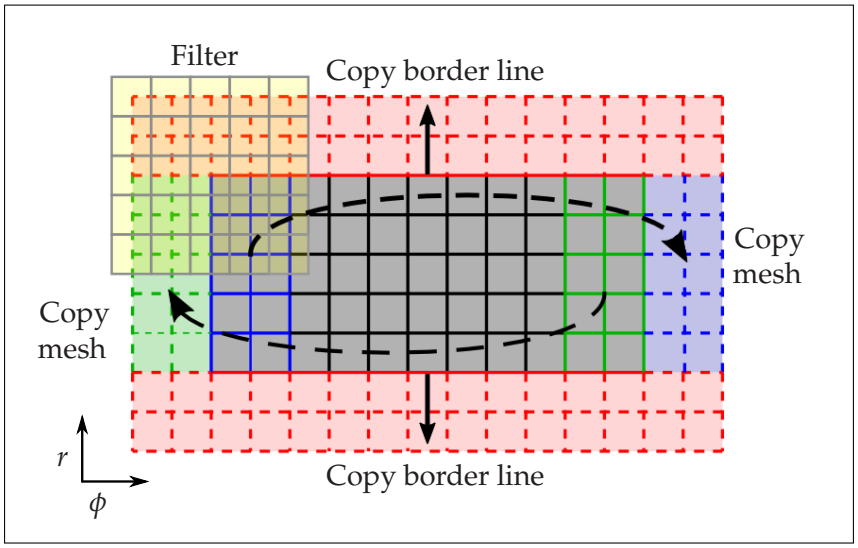

Figure 4.13: Extension of the mesh to prepare correct smoothing, filter order $n = 2$.

After applying the smoothing filter the added grid lines can be removed again. One disadvantage of applying a smoothing filter in the described way is the non-adaption of the Gaussian filter to the deformed circular shape of the actual measurement grid. For sake of simplicity the possible irregular grid line spacing is not accounted for either. But it has to be noted that the only purpose of the smoothing is the improvement of the visual quality of the picture and the errors caused by this kind of smoothing are usually too small to have any visual effect.

Only in the center of the loudspeaker it can happen that the data points vary in geometry and vibration due to the smoothing filter. To reach again a consistent behavior at the center with $r = 0$ an additional averaging of all center points is done after applying the smoothing.

In figure 4.14 the effect of differently sized smoothing filters on a noisy vibration picture is shown.

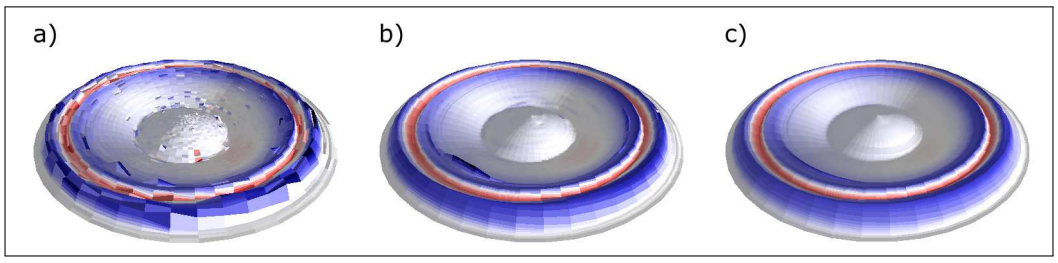

Figure 4.14: a) No smoothing, b) Medium smoothing, c) Strong smoothing.

The applied smoothing power is expressed by the standard deviation σ which describes the spatial influence of the Gaussian filter function. For the two dimensional Gaussian distribution 39.4% of the weighting amount can be found in a distance of σ around the center of the filter and 86.6% of the filter weighting lies in a distance of 2σ around the center. As σ is chosen in dependance of the filter order n the filter order will determine the spatial influence of the smoothing. To reach an approximatly constant radius of influence of the smoothing the filter order should be chosen according to the (average) grid spacing. Furthermore it is useful to let the user decide whether he wants to see a filtered picture of the vibrations and how large the smoothing radius should be by providing an accordant user interface.

4.1.3 Sound Radiation Modeling

On the basis of the measured vibration data a modeling of the radiated sound pressure is possible. As the produced sound is of final interest in the loudspeaker design a directly available model of the sound pressure is a helpful assistance. The sound pressure modeling is applied for two tasks, on the one hand the frequency response of the loudspeaker can be estimated at arbitrary model points and on the other hand the directivity of the loudspeaker is modeled at a chosen frequency.

Frequency Response

Several acoustical models can describe the relation between the velocity of a vibrating surface and the radiated sound pressure. These models differ regarding their accuracy and limitations.

The Rayleigh Integral is a simplified formulation of the more general Kirchhoff-Helmholtz Integral describing the sound field produced by arbitrary vibrating surfaces [Her 03], [Fra 75]. The Rayleigh Integral equation given in (4.10) provides a simple but exact representation for the sound radiation from a flat vibrating surface mounted into an infinite rigid baffle [Her 03].

$$p\left(\vec{R},\omega\right) = -\frac{\omega^2\rho_0}{2\pi}\int\limits_S \frac{e^{-jk_0\left|\vec{R}-\vec{r}_i\right|}}{\left|\vec{R}-\vec{r}_i\right|} x_n(\vec{r}_i)\; dS \tag{4.10}$$

with ρ_0 is the density in air, k_0 is the acoustical wavenumber in air, S is the surface area, $\left|\vec{R}-\vec{r}_i\right|$ is the distance between the surface point i and the model point and $x_n(\vec{r}_i)$ is the normal surface displacement at the point i.

The implemented sound radiation model places a monopole sound source at each measured point on the surface. The sound radiation contribution of one single surface point is illustrated in figure 4.15.

For the integration over the complete surface S of the measured cone it is necessary to sum up the sound radiation contribution of each surface point i weighted

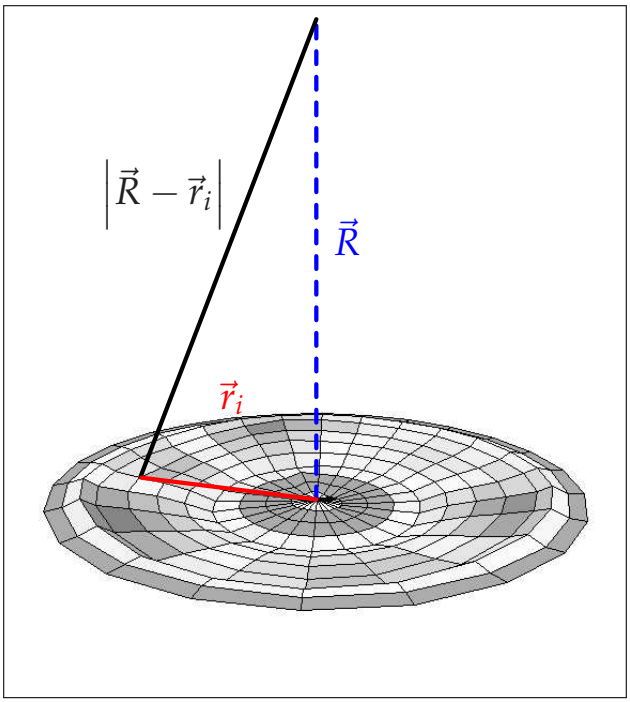

Figure 4.15: Sound contribution of surface point i.

with the respective area portion surrounding it. The surface elements $dS(i)$ can be approximated by ring sectors around i reaching half the way to the next adjacent measurement points in radial and angular direction, see figure 4.16

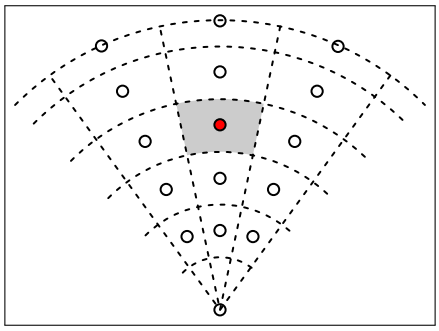

Figure 4.16: Area $dS(i)$ of the ring sector influenced by surface point i.

The surface elements in the center $r = 0m$ are circular sectors and the outermost ring sectors extend only until r_{max} to assure a correct representation of the complete measured cone surface.

Regarding the amplitude $\widehat{a}_x$ and phase ϕ_x of the measured displacement transfer function the integral in equation (4.10) can be evaluated numerically by the summation (4.11).

$$p\left(\vec{R},\omega\right) = -\frac{\omega^2\rho_0}{2\pi}\sum_r\sum_\phi \frac{e^{-jk_0\left|\vec{R}-\vec{r}(r,\phi)\right|}}{\left|\vec{R}-\vec{r}(r,\phi)\right|}\,\widehat{a}_x(r,\phi)e^{j\phi_x(r,\phi)}\cdot dS(r,\phi) \tag{4.11}$$

For the calculation of the frequency response the summation will be done over all surface points for each measured frequency. Considering the computational effort especially with a higher number of included measurement points the optimized matrix operations in Scilab can help to save much time.

There are a couple of assumptions under which the Rayleigh model is valid only, [Fra 75]. Firstly the loudspeaker is assumed to vibrate in an infinite rigid baffle. Furthermore only the sound pressure in the far field of the loudspeaker can be modeled, that means at points in a distance from the surface which is large compared to the considered acoustical wavelength in air. The model also neglects the influence of the moved air mass in front of the diaphragm which does have an effect especially at low frequencies.

Finally, the modeled sound pressure can only be valid for shallow cones and in particular not outside of the maximal opening angle of the cone because there is no diffraction around corners included in the model. The maximal valid opening angle θ_{max} is determined by the sound pressure modeling algorithm and model points outside this angular range are rejected, compare figure 4.17.

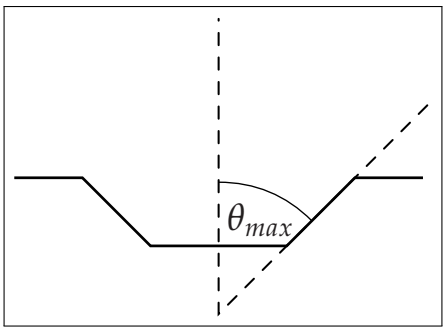

Figure 4.17: Maximal valid opening angle θ_{max} for sound pressure modeling.

The Rayleigh Integral method should provide a good approximation for a relatively flat surface as long as the higher amplitude vibration occurs in the center of that surface [Her 03]. This is true for the vibration of loudspeaker cones, therefore the surface modeling according to (4.11) promises a fair balance between accuracy and calculation speed. In section 5.1 an evaluation of the results of the sound pressure modeling algorithm will follow.

However, in case a higher precision of the sound pressure will become necessary it will be easy to replace the respective Scilab script with a more sophisticated method like the boundary element method (BEM) due to the separation of mathematical operations and visualization interface.

Directivity

The sound pressure modeling technique can also be used to calculate the directivity of the loudspeaker. For this the sound pressure is evaluated at one certain frequency for several listener points on a hemisphere around the speaker, compare figure 4.18

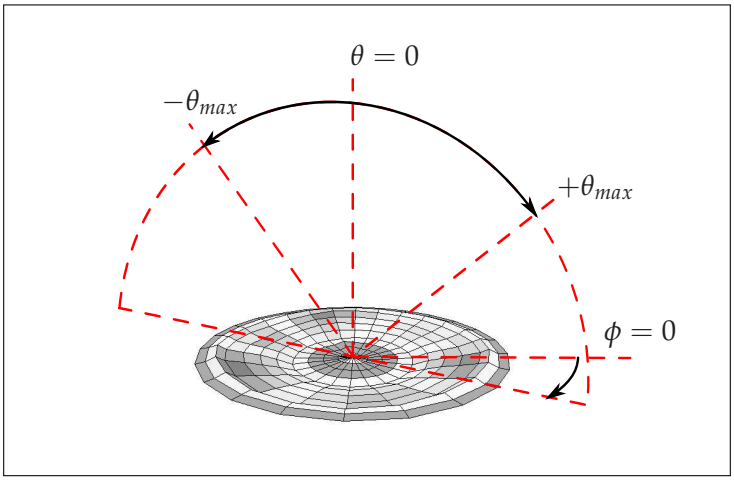

Figure 4.18: Listener points for the directivity plot.

Directivity plots can be used to analyze the spatial distribution of the sound radiation. A loudspeaker usually produces most of its sound output on a straight axis perpendicular to the cone. If the angle θ between this axis and the listener is different then the sound pressure is variating as well. It is very interesting for the speaker engineer to have control over the directivity because it is responsible for an even frequency response in a preferably big area.

Whereas directivity plots usually assume an axially symmetric radiation of the speaker, the implemented model allows to precisely look at a certain angle ϕ above the speaker surface to detect possible asymmetries in sound radiation.

In figure 4.19 the modeled directivity plots of an example loudspeaker at three different frequencies are shown. It can be observed that the measured loudspeaker has an omni-directional characteristic at 100Hz but it gets more and more directional at higher frequencies.

Special care has to be taken to mount the speaker exactly in the center of the turntable during the scanning process. Otherwise the accuracy of the directivity modeling is questionable especially at higher frequencies. One might see then laterally shifted directivity characteristics at high frequencies which do not represent the real behavior of the loudspeaker. See also 5.1 for an evaluation of the accuracy of the modeling method.

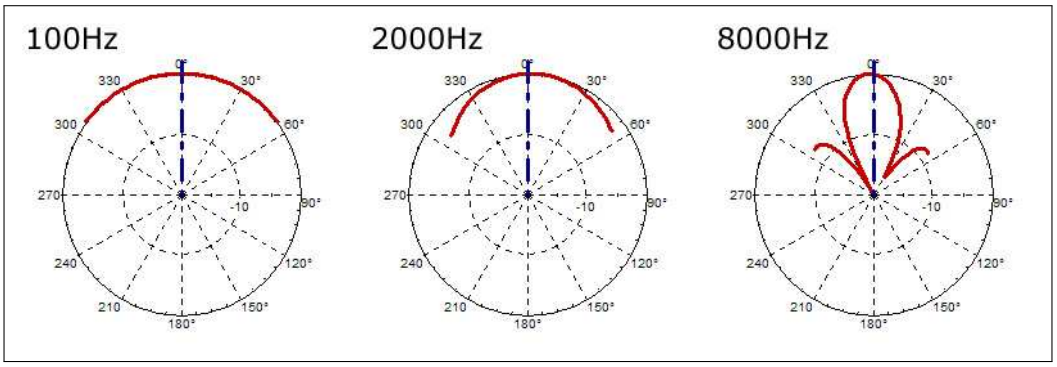

Figure 4.19: Directivity at different frequencies.

4.1.4 Data Decomposition

The intention of preprocessing the vibration data in order to provide useful analysis tools led to the idea of a decomposition of the complex vibration pattern into separate components with special relevance. Looking at a single component should provide a simplified picture on one special property of the loudspeaker vibration.

Two different decomposition techniques were developed, each approaching the problem from a different view. For the mechanical analysis of the cone vibrations a decomposition into radial and circumferential components can help to separate the influence of certain vibration modes. Another interesting analysis opportunity is to separate vibration components according to their relation regarding the finally radiated sound.

Decomposition of radial and circumferential Modes

A separation into vibration components propagating in radial direction and components propagating in circular direction is especially useful for axis-symmetric cones. Then both orthogonal propagation directions refer to independent mechanical vibration patterns, called modes, which do not interfere with each other. The superposition of the radial component x_{rad} and the circumferential component x_{circ} results in the total vibration, see (4.12).

$$x_{tot} = x_{rad} + x_{circ} \tag{4.12}$$

Theoretically, circumferential vibrations should hardly occur in axis-symmetric loudspeaker cones, because they are not excited by a symmetrically moving voice coil. But in practice small irregularities will also lead to some circular motions in the cone. This component is usually quite small in comparison to the radial motion and might therefore be hardly visible looking only at the total vibration. See figure 4.20 for an example decomposition at 375Hz.

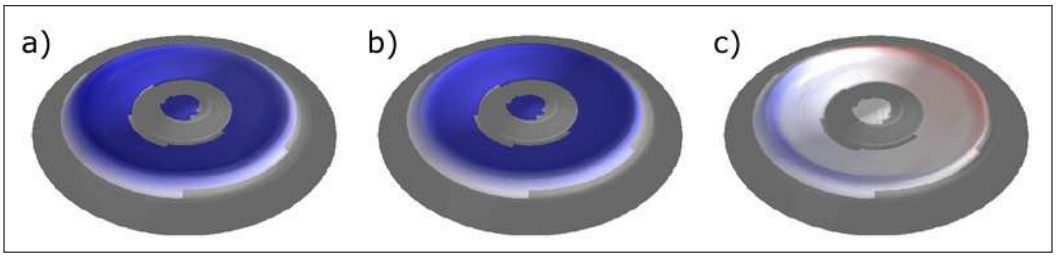

Figure 4.20: a) Total vibration, b) Radial component, c) Circumferential component.

The decomposition is implemented by an averaging over the n vibrating points at angles ϕ_n along each radius on the cone surface. Projecting this average value on all points along the respective radius results in the radial vibration component x_{rad}, see (4.13).

$$x_{rad}(r,\phi) = \frac{1}{n}\sum_{i=1}^{n} x_{tot}\,(r,\phi_i) \tag{4.13}$$

The remaining circular vibration component is obtained by subtracting the radial component from the total vibration (4.14).

$$x_{circ}(r,\phi) = x_{tot}(r,\phi) - x_{rad}(r,\phi) \tag{4.14}$$

According to Frankort [Fra 75], the circular vibration components have a negligible effect on the total radiated sound. Therefore the simplification of the vibration picture by considering only the radial component should maintain the sound radiation properties while showing an easier understandable picture of the cone vibrations, see figure 4.20 b)

On the other hand considering only the circular vibration component can reveal asymmetric vibrations, see figure 4.20 c). While not contributing much to the radiated sound these components can nevertheless cause distortion due to rubbing of the voice coil in the gap. The reason for asymmetric vibrations can be a non-symmetric mass distribution of the voice coil or the cone, which can be recognized and quantified by this analysis tool.

Furthermore the circular components can still have some effect on the sound pressure considering radiation regions aside the central loudspeaker axis. A circular cone vibration mode will usually lead to a multipole (dipole, quadrupole,...) radiation pattern with little radiated sound pressure in axis but radiating side lobes.

It has to be noted that this kind of vibration decomposition presumes an accurate centering of the speaker on the turntable. Otherwise there might occur artifacts in the circumferential component which pretend some circular vibration, but originate from radial components being measured in a radially not centered grid. Therefore the circumferential components have to be regarded with care especially

at higher frequencies where bending waves with short wavelengths appear on the cone.

Sound Pressure related Decomposition

A second form of decomposition can be utilized to identify the regions on the loudspeaker which effectively contribute to the total radiated sound pressure at a certain model point. The idea is to separate a vibration component which supports the sound radiation from a component which counteracts the sound vibration and a component which has no effect on the radiated sound at all.

The criterion to distinguish these three components is the phase relation between the vibration of each point on the cone surface and the total sound pressure at the model point. The vibration can be aligned with the total sound pressure in-phase, in anti-phase or out-of-phase. The superposition of the three respective vibration components produces again the total vibration, see (4.15).

$$x_{tot} = x_{in} + x_{anti} + x_{out} \tag{4.15}$$

The phase of the displacement $\phi_x(i)$ at each point i on the surface is set in relation to a reference phase $\phi_{ref}(i)$ starting from the phase of the total sound pressure ϕ_p and including the time delay for the acoustical wave having traveled from the cone surface to the model point (4.16), compare also figure 4.15 on page 42.

$$\phi_{ref}(i) = \phi_p + k_0 \left| \vec{R} - \vec{r}_i \right| + \pi \tag{4.16}$$

The term $k_0 \left| \vec{R} - \vec{r}_i \right|$ in (4.16) refers to the time delay and the additional phase shift of π origins from the phase difference between the displacement and the acceleration of the surface. The acceleration of an infinite vibrating plane is directly proportional to the sound pressure at the plane and therefore the acceleration would be everywhere exactly in-phase with the radiated sound pressure.

An in-phase contribution describes now the positively related component between the phase of the displacement $\phi_x(i)$ at each point i and the reference phase ϕ_{ref}. Accordingly the anti-phase component is the negatively related component and the out-of-phase component describes the component perpendicular to the total sound. The respective relations are derived from the vectorial relations of the phases in the complex number plane, compare figure 4.21.

The relation between ϕ_{ref} and ϕ_{x1} results in an out-of-phase component and a smaller in-phase component while ϕ_{x2} is strongly in anti-phase to ϕ_{ref}. The mathe-

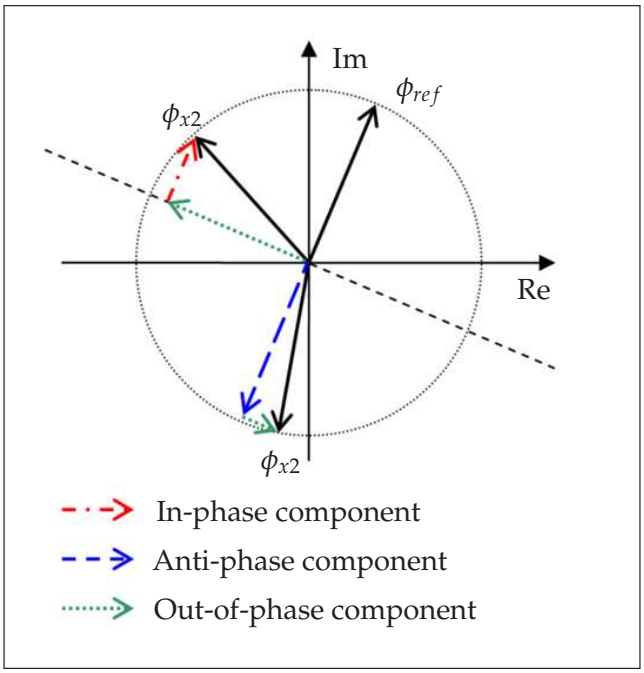

Figure 4.21: Phase relations for SPL decomposition.

matical description of the actual decomposed vibrations is given in (4.17)

$$x_{in} = \mathrm{Re}^{+}\left\{ a_x \frac{e^{j\phi_x}}{e^{j\phi_{ref}}} \right\} e^{j\phi_{ref}} \tag{4.17a}$$

$$x_{anti} = \mathrm{Re}^{-}\left\{ a_x \frac{e^{j\phi_x}}{e^{j\phi_{ref}}} \right\} e^{j\phi_{ref}} \tag{4.17b}$$

$$x_{out} = \mathrm{Im}\left\{ a_x \frac{e^{j\phi_x}}{e^{j\phi_{ref}}} \right\} e^{j\left(\phi_{ref}+\frac{\pi}{2}\right)} \tag{4.17c}$$

Having the possibility of decomposing the vibrations with respect to their contribution to the radiated sound offers many opportunities for analyzing the behavior of the measured loudspeaker. An example analysis of a measured loudspeaker using the here introduced decomposition techniques will follow in 5.2.

4.2 Graphical Presentation

All the functionality described in the previous section 4.1 has to be combined under a common user interface giving quick access to the different measurement analysis opportunities. The visualization application developed for this task includes a project management organizing the settings and files of the respective scanning projects, different graphical components and plots illustrating the post-processed

measurement results and various opportunities to export the results to external applications.

After opening an existing scanning project the visualization application offers a clearly arranged interface, see figure 4.22. The screen is divided into a graph of the

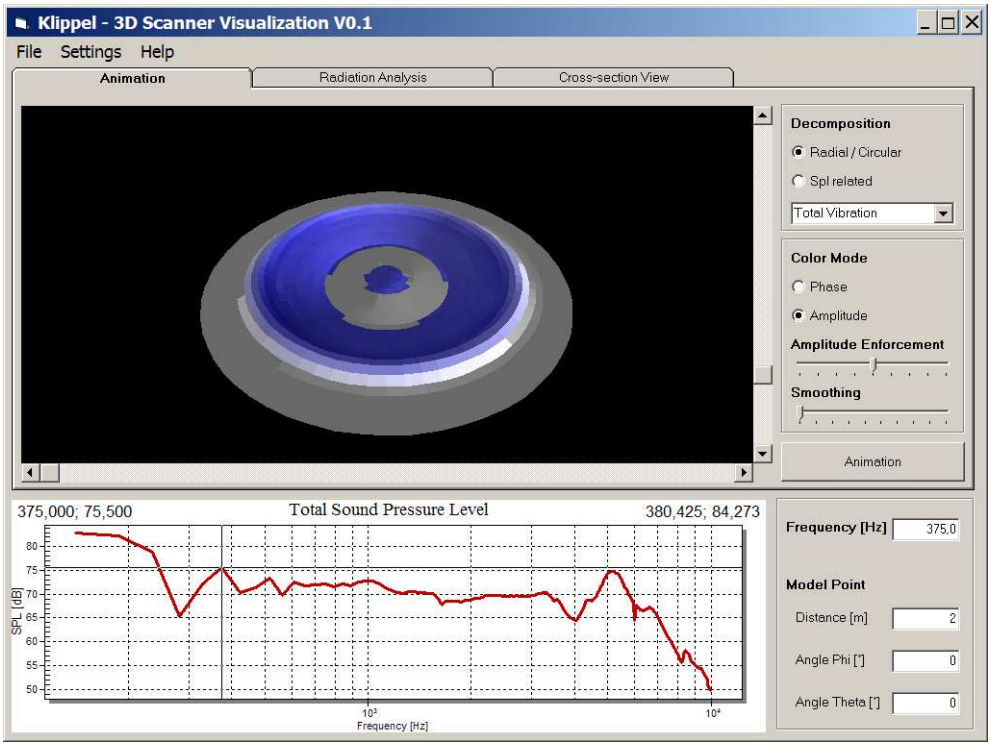

Figure 4.22: Visualization application with 3D picture of the measured loudspeaker.

modeled frequency response at the bottom and different vibration analysis graphs arranged in three tabs in the upper screen part. A menu offers access to file related actions like opening scan projects and exporting results, to general settings and a small help.

The frequency response serves as navigation tool to select the current analysis frequency. It provides a quick overview over the loudspeaker performance and problematic peaks and dips which require a closer investigation. Also a text-based input of the frequency and the exact position of the model point can be found right to the sound pressure plot.

The frequency response is calculated once while loading the scanning project and it has to be recalculated each time the model point is changed or one of the decomposition techniques is applied. The modeled frequency response results can be cached in the VB application to avoid unnecessary recalculations, but up to now the caching is only implemented for the different vibration components at one certain model point.

Three different analysis tabs can be chosen, firstly a 3D animation of the vi-

bration, secondly a radiation analysis with a directivity plot and thirdly a two-dimensional animation of a cross-sectional cut through the loudspeaker.

4.2.1 3D Animation of the Vibrations

The animation is realized by using a Pro Essentials 3D Object (Pe3do) provided by the PeGraph ActiveX package from Gigasoft, see section 3.2.

From the measured geometry of the loudspeaker a 3-dimensional surface of the cone can be created. This surface serves as rest position and the amplitude of the vibration is displayed as an offset superposing the geometry including a certain scaling to emphasize small movements.

The interpolation algorithm introduced in section 4.1.1 is used to properly fill up the missing data points. Each time a different frequency or a different vibration component is chosen, the interpolation algorithm has to be started again. Also a different smoothing parameter or a different number of visualization points require a recalculation of the interpolated picture.

Different coloration schemes were developed to offer appropriate illustrations for the user. It is possible to quickly switch between these coloration schemes by choosing the respective option in the settings frame next to the 3D animation.

A first way of coloration is based on the amplitude of the vibration. A positive amplitude is correlated with a blue color and a negative amplitude with a red color while neutral points remain white. The intensity of the coloration expresses the magnitude of the vibration in relation to the amplitude on the complete surface at the respective chosen frequency. That means the point with the highest amplitude will be colored in dark blue or red while a point with little amplitude will get only a lightly shimmering blue or red tone. A quadratic curve mapped in the RGB color space (red, green, blue) establishes a smooth transition from dark red to white and then to dark blue, compare figure 4.23.

The average root mean square (RMS) value of the vibration amplitude a_{rms} helps to adjust the color scale. It has been found an useful approach to set the limits of the color scale to plus/minus two times a_{rms}. Single vibration values outside these limits are clipped to the respective limit. These outstanding vibration points are most probably erroneous and the clipping and dark coloring helps the user not being distracted by them.

An additional optical enforcement of the amplitude was implemented to emphasize smaller vibration levels. The color scale as well as the animation amplitude can be manually adjusted to the actual preferences of the user by shifting the nominal a_{rms} up or down.

In an alternative coloration scheme only the phase of the vibration determines the color. A phase angle of $\phi_x = 0$ now corresponds to the color yellow and the opposite phase of 180° is represented by a red color, see figure 4.24.

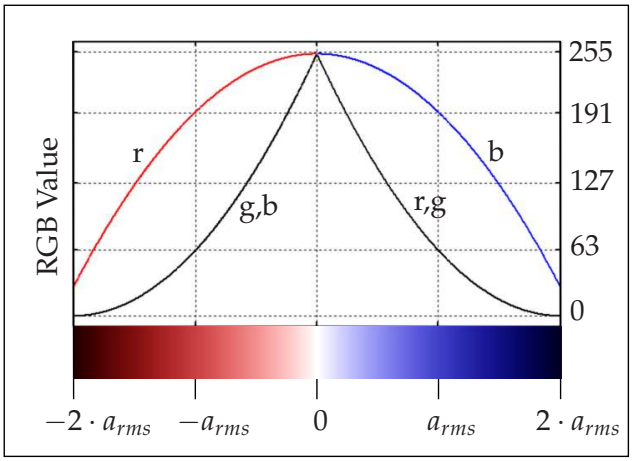

Figure 4.23: Color transition of amplitude coloration.

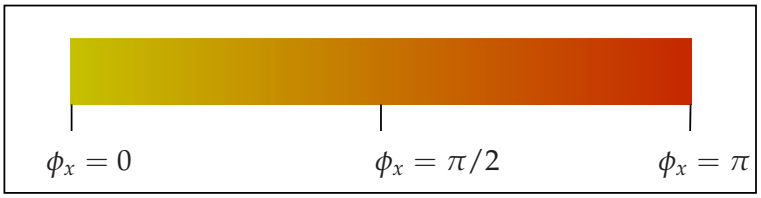

Figure 4.24: Color transition of phase coloration.

In between these both phases a smooth color transition is established. The advantage of this coloration is that even vibrations of small amplitude will be clearly visible. The spatial shape of the vibration pattern appears more clearly which helps to determine the involved vibration modes. In figure 4.25 both coloration schemes are shown for an example loudspeaker.

All points where the laser could not measure vibration data are indicated by a neutral gray color to emphasize that these points are only interpolated and may not exactly represent the actual vibration.

A second version of both coloration schemes is realized in a monochrome way to support the printing of certain pictures in black and white. Here the phase coloration extends from white to dark gray while the amplitude coloration is less clearly interpretable because positive and negative amplitude are colored dark gray and zero amplitude equals white again, see figure 4.26.

Animation as a stroboscopic Movie

A graphical animation can illustrate the behavior of the cone vibrations in a very good way. If single pictures are displayed at a rate higher than about 24 frames per second (FPS), then the human eye interprets the picture sequence as a continuous

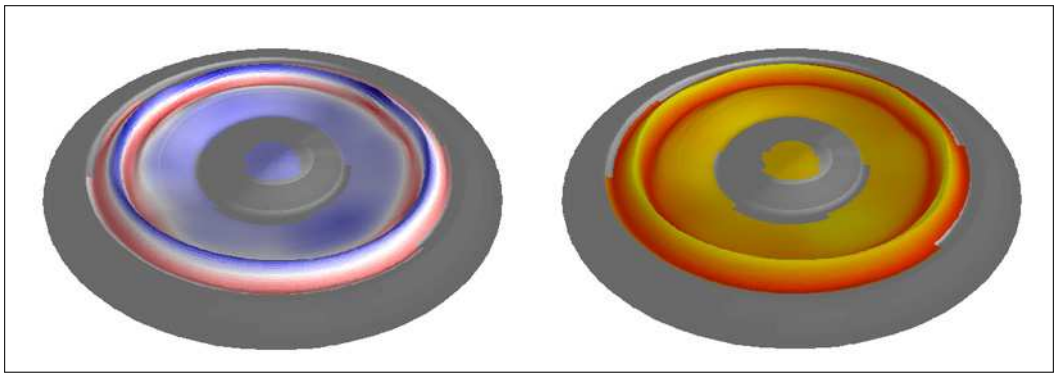

Figure 4.25: Amplitude and phase coloration of an example speaker at 2kHz.

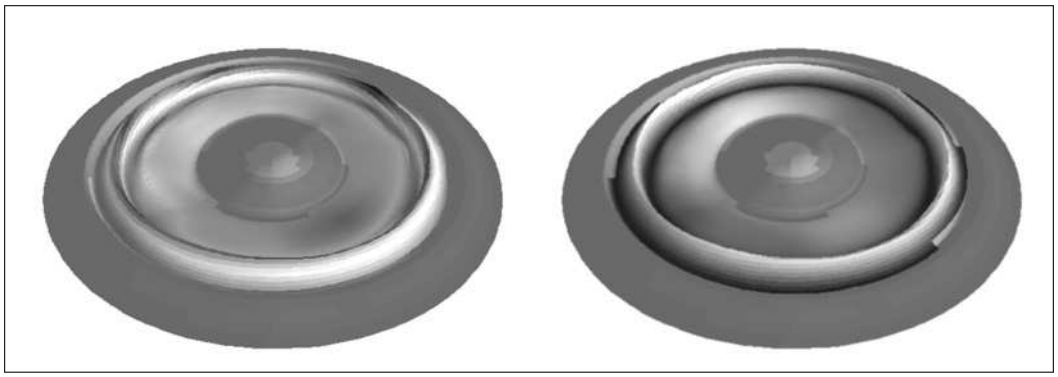

Figure 4.26: Monochrome amplitude and phase coloration at 2kHz.

motion. One way of animating a vibration is to rotate the phase angle of all points by 360° during one animation period. The period time T can be chosen freely to slow down the vibration until a good understanding of the animation is possible.

To calculate the single frame number n of the animation for each point on the 3D surface the phase ϕ_x of the displacement transfer function h_x has to be changed by small steps according to (4.18).

$$h_x(n) = \widehat{a}_x \, e^{j\left(\phi_x + \frac{2\pi T}{FPS} n\right)} \tag{4.18}$$

Obviously this calculation can become quite time-consuming the more points have to be recalculated. If the calculation of the frames takes more time than the animation frame rate allows, a visible delay and flickering in the animation will occur. Furthermore the used 3D graphics engine from PEGraph is only able to produce real-time animations of objects up to a number of about 2500 vertices, compare section 3.2. Therefore a compromise has to be found between the number of displayed points and a fluent animation.

This restriction can be circumvented by calculating all necessary pictures first and then creating a movie file from the calculated pictures. Now the calculations

do not have to be done in real-time and also a higher number of points can be used while keeping a fluent animation, see section 4.2.5 for the description of the movie export.

The vibration of the loudspeaker cone can be decomposed using the methods introduced in section 4.1.4. A decomposition will effect the animation as well as the sound pressure modeling. In that way not only the spatial structure of the vibration, but also the radiated sound of single components can be evaluated. An option right next to the animation graph can be used to select the actual vibration component or to look at the total vibration.

While using the amplitude coloration scheme with single components the colors will be scaled in reference to the total vibration. That means the relations of the single components in comparison to the total vibration remain constant and can be compared. The application of these decompositions will be shown for an example loudspeaker analysis in section 5.2.

4.2.2 Radiation Analysis

In the second tab of the visualization analysis software there can be found a graph to evaluate the radiation properties of the loudspeaker with the help of directivity plots, see figure 4.27. All options from the previous tab can also be found here except the animation button which is redundant here. Again a data decomposition can be applied to focus on a certain vibration component.

Two graphs next to each other in the upper region of the screen can be used to choose the angles θ and ϕ describing the model point of the sound pressure modeling in spherical coordinates. The right graph shows a top view of the actual 3D vibration graph from the previous tab. A white line crossing the picture is used to indicate the currently selected angle ϕ and can be moved by clicking on the graph.

The left graph shows the modeled directivity plot for the actual frequency and vibration component. The directivity is shown normalized to its maximum which means the maximal radiation direction at a certain frequency is set to $0dB$. The actual angle θ of the model point is shown and can be changed by a blue line in the directivity graph.

Each time the angles θ or ϕ are changed, the model point changes and the sound pressure plot in the bottom is recalculated. The combination of sound pressure plot and directivity plot provides a complete picture of the radiation properties of the measured cone.

4.2.3 Cross-section View

The last tab in the visualization software contains a two-dimensional view of the vibrations along a cross-sectional cut through the loudspeaker, see figure 4.28. The

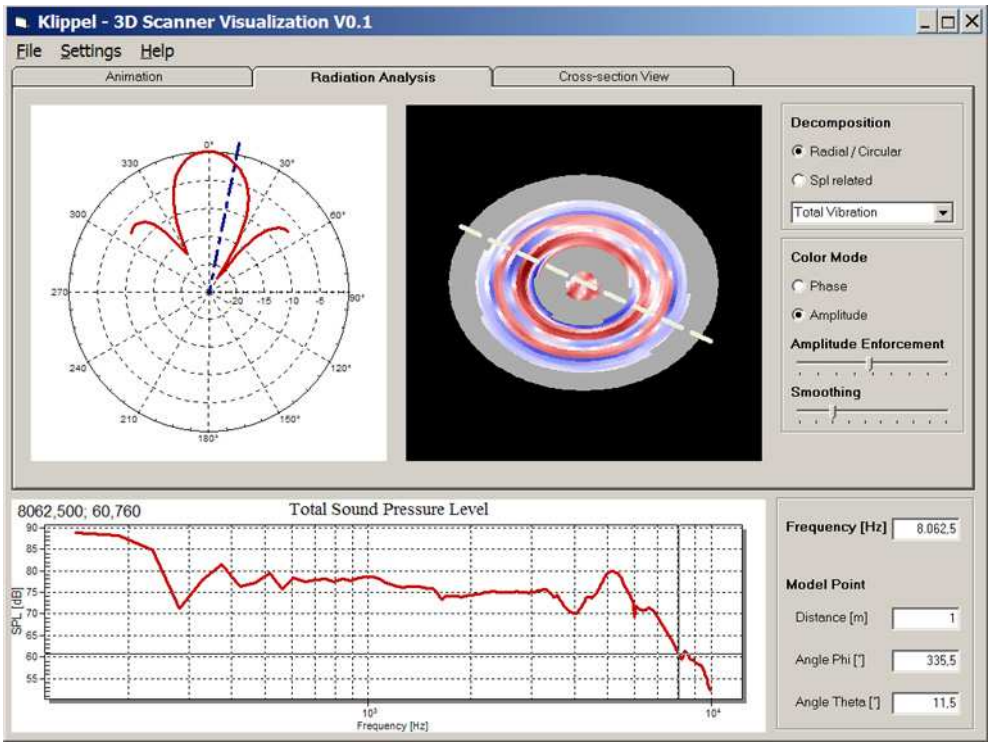

Figure 4.27: Radiation analysis screen-shot.

two-dimensional view is sometimes easier to interpret, especially if higher order bending modes are apparent on the cone surface. Furthermore the view is more appropriate for determining the exact positions of vibration maxima and nodal points where the amplitude is almost zero.

The angle ϕ selected for the model point of the sound pressure modeling also determines the angle of the cut line through the speaker. Therefore the cut line can be easily selected in the right picture of tab two and the vibration along this selected cut can be examined in tab three.

All options for the 3D animation like decomposition, smoothing and amplitude enforcement apply as well for the two-dimensional graph. It is also possible to animate of the cross-cut line to examine the vibration.

4.2.4 Settings

The settings are divided into application related and project related settings, see table 4.2.4. As the name already implies, the application settings apply for all projects whereas project settings are saved together with each scanning project. The visualization application shares the same setting files with the scanning software to support an easier integration of both parts in future.

The application settings of the visualization software can be accessed over the

Figure 4.28: Cross-section view screen-shot.

menu. There it is possible to choose a language file which contains all strings of the user interface in a localized version. Also the content of error messages is localized using this language file. By simply exchanging the text-based file the complete application can be adapted to the preferred language. During the development of the visualization software an English and a German version were created and there might be the demand to include more languages in future.

Two settings of the animations were also referred to this extra dialog box. On the one hand the period time T of the animation describes the animation speed which might not be changed too frequently. A period time of $1.5s - 2s$ creates well understandable pictures of the vibration and only in some cases an even slower animation might give more insight into the vibrational behavior.

On the other hand one can also find the number of maximal visualization points here in the settings menu. Tests of the graphics engine showed a fluent animation behavior up to about 2500 points, see section 3.2 page 26. However an animation is of course also possible for a higher number of points and although the animation will not be fluent anymore, pictures of higher quality can be produced in this way. To also get a smooth animation for a very high number of visualization points the movie export function can be used, see section 4.2.5.

The project settings represent mainly the current analysis state. While closing a project the user is asked whether he wants to save these settings to a file. Like this

Application settings	Project settings
Language file	Frequency
List of recently opened projects	Model point
Animation period time	Active tab
Number of visualization points	Color mode
	Smoothing
	Amplitude enforcement
	Vibration component

Table 4.1: Classification of the settings.

it is possible to continue the vibration analysis at the same position the next time the project is loaded.

4.2.5 Data Export Opportunities

An important requirement for the visualization software is offering the opportunity to transfer the results to external applications. This can be useful for a further analysis of the data or for a comparison with results from finite element programs. Also a persistent storage of certain interesting graphs and animations can be helpful to track the effects of changes in the loudspeaker design.

Picture Export

The used graphics components from PEGraph provide a variety of built-in picture export functions. All diagrams and still pictures of the vibration animation can be copied to the Windows clipboard or saved in a file. Available picture formats are the vector graphics format EMF from Microsoft, the bitmap graphics format BMP and two compressable graphics formats JPG and PNG. Thereby the nominal size of the target pictures can be freely chosen and by this also high quality raster images can be created, see figure 4.29.

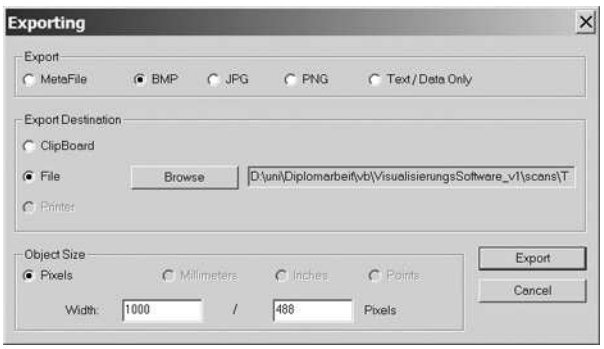

Figure 4.29: Built-in picture export menu.

The picture export is accessible via an entry in the context menu appearing while clicking on the respective graph. The standard context menu predefined for each PEGraph component can be adapted to the special requirements of the visualization software.

Geometry Export

The measured geometry of the loudspeaker cone can be a very useful input for many Computer Aided Engineering (CAE) programs. To offer the possibility of exporting the three dimensional surface mesh of the measured cone geometry the common drawing interchange format (DXF) originally developed by Autodesk® [Aut 98] is used.

The geometry of the already interpolated mesh can be exported in the DXF format by specifying the x, y and z coordinates of each vertex. Four vertices are combined to one 3d-face data construct. Some additional header informations complete the specification of a simple DXF file containing the geometry information of the measured cone.

It has been possible to successfully import the created files into various DXF compatible applications like the freely available DXF Viewer and the current version of AutoCAD 2007 by Autodesk.

Movie Export

The export of a 3D animation into a movie file serves two different intentions. On the one hand a movie file is the best method to conserve the vibrational behavior for presentation purposes and for a comparison with subsequent measurements. On the other hand due to the fact that the calculations of the involved pictures do not have to be done in real-time a fluent animation can be assured even for a very high number of visualization points.

A separate dialog is used to define all settings concerning the export of an animation as a movie file, see figure 4.30. The current animation from the first tab of the main software frame is reproduced in an enlarged form and various animation parameters can be chosen separately for the export of the current movie.

At first the height and width of the final movie can be defined according to the purpose of the movie. Also the graphical quality of the animation can be refined by setting a higher number of visualization points and an appropriate smoothing degree. The period time can be set accordingly to slow down the animation to the desired degree.

The frames per second should be set to 25 to realize a fluent animation, but can be chosen higher or lower if desired. It is also useful to save more than one loop of the animation to get a better impression of the vibration behavior. The single movie frames will then be saved as temporary picture files in the given format.

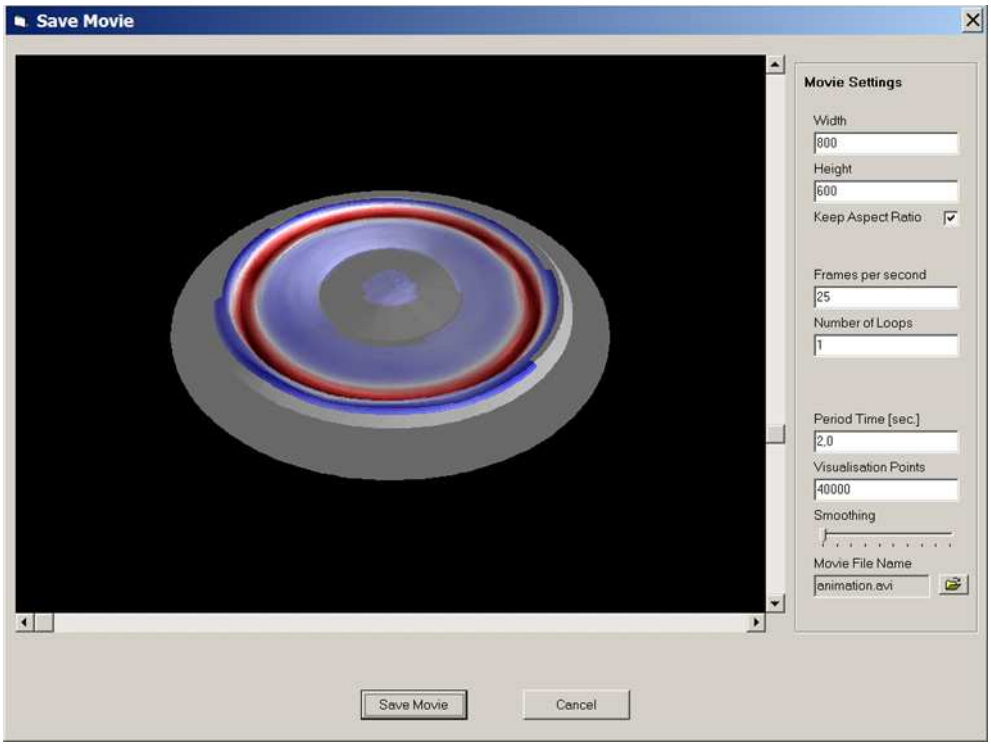

Figure 4.30: Movie export dialog.

The looping pictures are not calculated again, but will only be put again in the created video stream.

When the movie export is started by clicking on the *Save Movie* button, the single movie frames are each calculated and saved in a temporary bitmap file. Afterwards the bitmaps are combined to a video stream using the AVI movie container format. The movie compression method for the AVI file can be chosen among the currently installed codecs. A number of different video codecs is already provided with each standard installation of Microsoft Windows.

The compressed video file can be opened in an arbitrary video viewer application like the Microsoft Media Player or the DivX Player software.

Export of Modeling Results

The result plots of the sound pressure modeling can be interesting to import into external applications for instance for comparison with actual measurements or former modeling results. The PEGraph components also offer a text-based export of the displayed data curves. But this text export does not comply too well with the respective input functions for instance in Microsoft Excel, Matlab or Scilab which are commonly used applications for further analysis steps. Therefore the data export of curve data has been reimplemented to reach an easier interaction with the

preceding applications.

Basis of the text based export of the sound pressure modeling graphs is the commonly used Matlab file format which can be easily imported in Scilab as well. Furthermore the Klippel Distortion Analyzer, the basic measurement hardware for the vibration measurement, is delivered together with an analysis software which can import such Matlab text files from the clipboard and display the curves in various ways.

As the Distortion Analyzer is anyway necessary to conduct the vibration measurements, it is a convenient procedure to copy the result curves from the visualization application into the analysis software of the Distortion Analyzer. There the data curves can be compared and saved in a data base. Also a comparison of sound pressure modeling and true sound measurements can be realized in this way and the accuracy of the modeling technique can be evaluated as in section 5.1.

An extra interface for exporting the vibration data is not implemented up to now. For this the Scilab script used for the data interpolation could be adapted to save the results in an additional file before transferring them back to the visualization application.

5 Evaluation

5.1 Experimental Validation of the Calculations

The sound pressure modeling method as implemented in the visualization software is based on a number of assumptions which are not perfectly fulfilled for the actual sound radiation from a loudspeaker cone, see section 4.1.3 on page 41. Therefore an experimental validation of the implemented model was conducted to investigate the reliability of the modeled sound pressure plots.

An example loudspeaker was scanned with the laser scanner using a high spatial resolution and the results of the modeling algorithm are compared with real sound pressure measurements.

The measurement setup was chosen in order to comply with the assumptions of the sound modeling as much as possible. That means, the loudspeaker was measured outdoors and placed inside a big box on the ground facing upwards, see figure 5.1 for the setup.

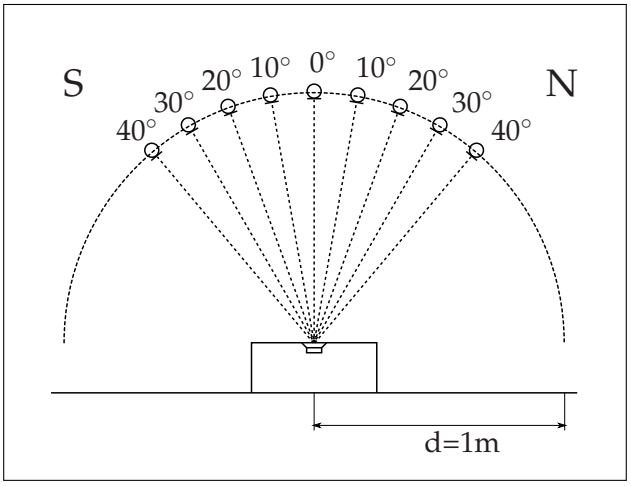

Figure 5.1: Setup for measuring the radiated sound pressure.

One assumption of the model is that the speaker is placed in an infinite rigid baffle. The used box is of course not infinite but chosen large enough in comparison to the wavelength of sound in air that the assumption is sufficiently well represented for higher frequencies. A better solution would have been to mount the loudspeaker directly on the same level as the surrounding ground, but unfortunately this was not possible.

It was also not possible to completely avoid the influence of reflections on the measured sound but the closest reflecting house wall was about 4 meter away from the measurement setup. To get more accurate measurement results it wold be advisable to conduct the experiment again in an anechoic or semi-anechoic chamber.

The measurements were conducted using the Klippel Distortion Analyzer device. A sinusoidal frequency sweep from 20Hz to 10kHz was used at an input voltage of 1V. Each measurement has been repeated 32 times per microphone position to reduce the influence of exterior noise on the results. The microphone positions were adjusted to a distance d of 1m from the center of the loudspeaker and measurements were taken first in axis and then for different angles θ to also evaluate the modeling of the directivity, see figure 5.1.

In figure 5.2 the results of both the sound measurement and the modeled sound pressure level in axis can be seen. The resolution and frequency range of the measured curve is adapted to the modeled curve.

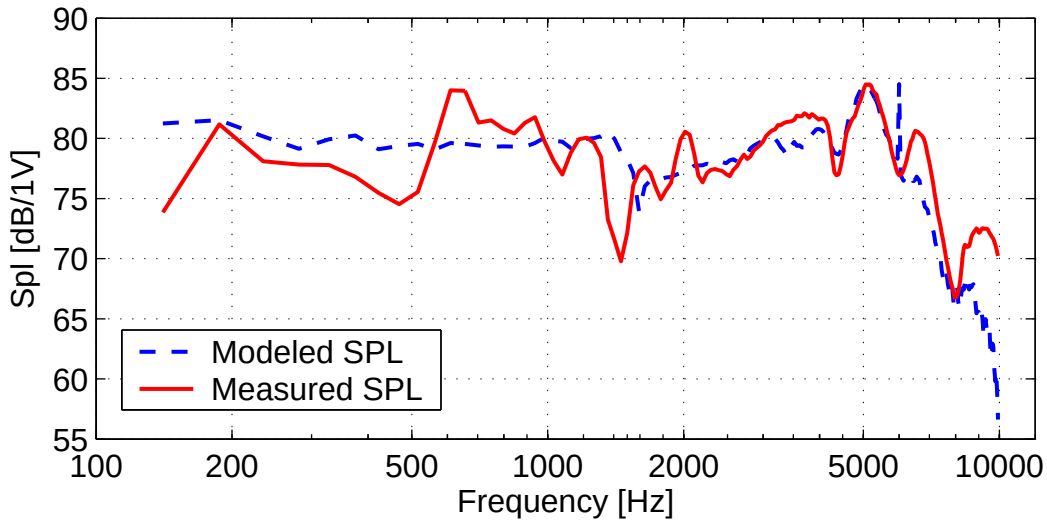

Figure 5.2: Sound pressure level in axis, $\theta = 0°$.

The modeled curve does not coincide perfectly with the measurement, but quite a good agreement can be seen especially in the range from 2kHz to 8kHz. The distinctive dip in the measured loudspeaker response at 1.5kHz is slightly shifted upwards to 1.6kHz in the model and not as deep. On the other hand the strong peak at 5kHz can be found identically in model and measurement data. In any case, the general shape of both plots agrees adequately well so that the sound pressure modeling can give valuable information about the true sound radiation.

In the lower frequency range especially around 400Hz to 700Hz the difference between model and measurement is larger. A reason for this might be the not optimal measurement setup with the mounting of the speaker in a box rather than in a large baffle leading to edge diffraction effects. The lower validity limit of the

used sound pressure model should be determined again by measuring the speaker response mounted in a large baffle in an otherwise anechoic environment.

The plots for different angles θ can be seen in the figures 5.3 to 5.6.

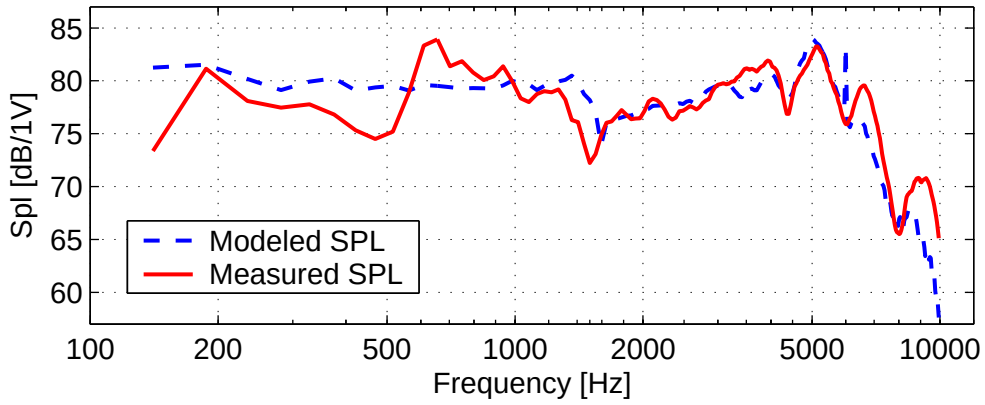

Figure 5.3: Sound pressure level for $\theta = 10°$.

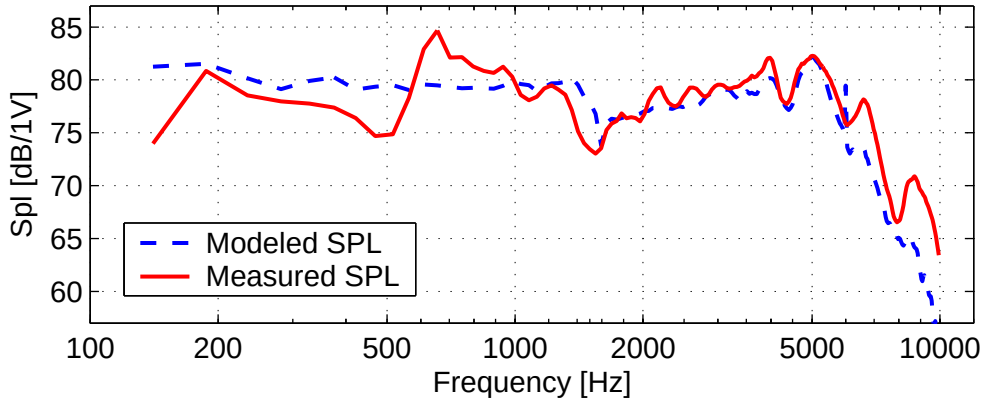

Figure 5.4: Sound pressure level for $\theta = 20°$.

These plots are created each by averaging 4 measurements and modelings for chosen angles ϕ of 0°, 90°, 180° and 270°. Although possible irregularities in the directivity can not be recognized in this way, the general behavior of the sound pressure model at arbitrary angles θ can be evaluated more easily. The measurement setup and conditions were not accurate enough to reproduce the same asymmetric directivity as in the models. But of course also the sound measurements showed significant deviations among the four different angles ϕ.

The agreement between measurement and modeled sound pressure level is very good for all the figures 5.3 to 5.6. A distinctive spike at exactly 6kHz can be seen in all modeled sound pressure plots. This spike results most probably from problems with the vibration measurement hardware and effort is taken to remove this

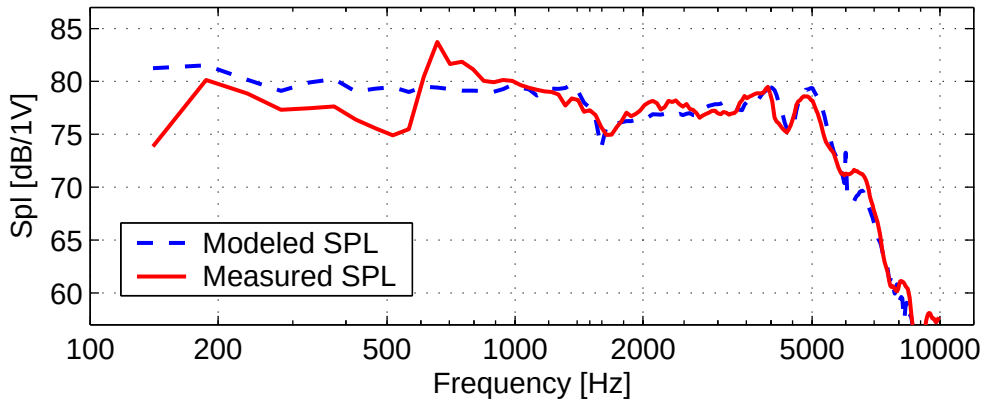

Figure 5.5: Sound pressure level for $\theta = 30°$.

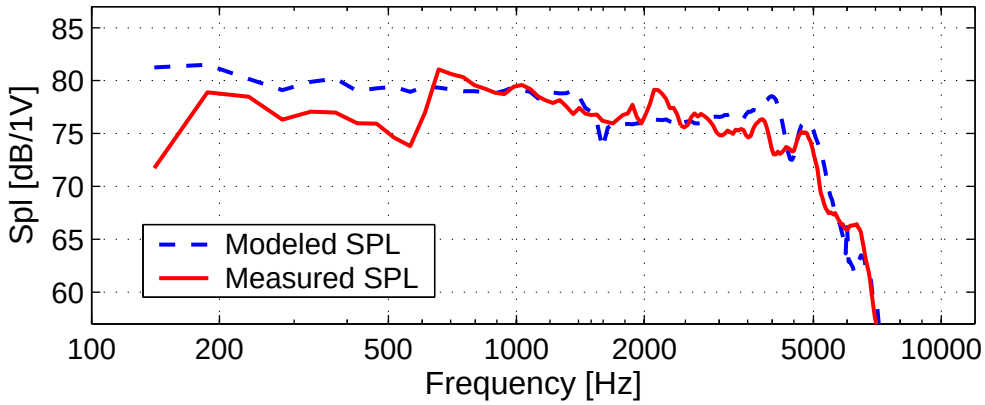

Figure 5.6: Sound pressure level for $\theta = 40°$.

physically non-existing peak from the vibration data.

To realize a directivity plot as shown in the visualization application would need more measurements in a finer angular resolution for θ. The measurements were taken only at a few angles θ but over the complete frequency range which also gives a good indication of the accuracy of the complete directivity plots. In figure 5.7 the comparison of one modeled directivity plot with the measurements is shown for the frequency of 5kHz. The measurements, indicated by the crosses in figure 5.7, agree very well with the modeled curve. The directivity models are not always as accurate as the shown plot at 5kHz, but they mostly show the right shape of the curve within only a few dB deviation.

In conclusion the sound pressure modeling based on the Rayleigh Integral approximation works fairly well for the prediction of the sound field produced by a shallow loudspeaker cone. Not all details of the actual radiation are predicted with high precision, but the general shape of the frequency response at arbitrary listener points in the far field is represented sufficiently accurate for many applications. If a

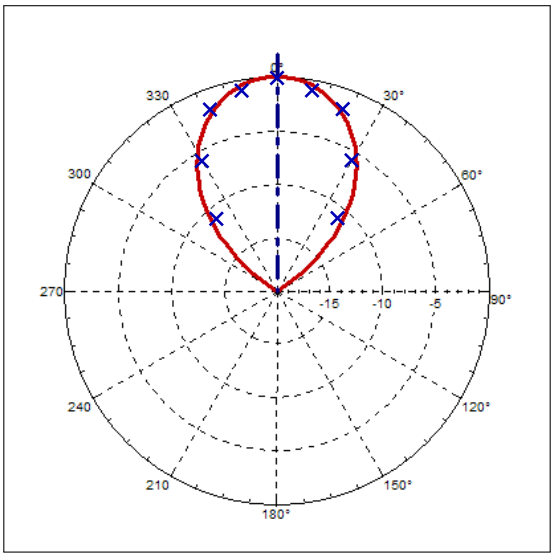

Figure 5.7: Measured and modeled directivity at 5kHz.

higher prediction accuracy of the sound pressure modeling is required for a special application, then it is possible to exchange the modeling script in Scilab by a more sophisticated modeling technique like the boundary element model (BEM).

5.2 Analysis of an Example Loudspeaker

In this section the visualization software is applied for demonstrating an analysis of the vibration and radiation of an example loudspeaker. The theoretical behavior of the loudspeaker according to [Fra 75] is illustrated and evaluated at different frequencies. The vibration of loudspeaker cones is generally characterized by a in-phase vibration of the complete cone at low frequencies and the occurrence of more and more bending vibrations at higher frequencies.

Piston Mode

At low frequencies most of the points of the cone vibrate in phase and there are no waves on the cone surface propagating in radial direction, see figure 5.8. That means the complete cone is moving back and forth as one rigid surface. In the 3D animation as well as in the animation of the cross-cut a uniform up and down motion of the complete cone is visible.

However, circumferential modes can be found at frequencies where a circular path is exactly two or more wavelengths long. Since the bending stiffness of the outer cone suspension, also called surround, is much smaller than the stiffness of the cone the first circular waves usually occur on the surround at very low frequencies.

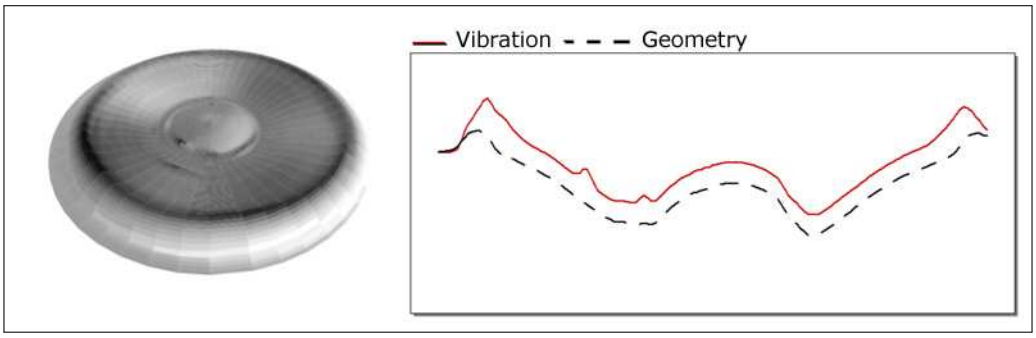

Figure 5.8: Amplitude of the total vibration at 580 Hz.

Because the vibration amplitude of the piston mode is still dominant the decomposition technique is required to make smaller circular modes visible. In figure 5.9 the phase of the vibration component is shown which is acoustically short-circuited and does not contribute to the sound pressure at the measurement point (1 m, in axis). This out-of-phase component contains only circular modes which generate black and white spots of similar size vibrating with opposite phase. Here the phase coloration is more suitable to emphasize the vibration pattern.

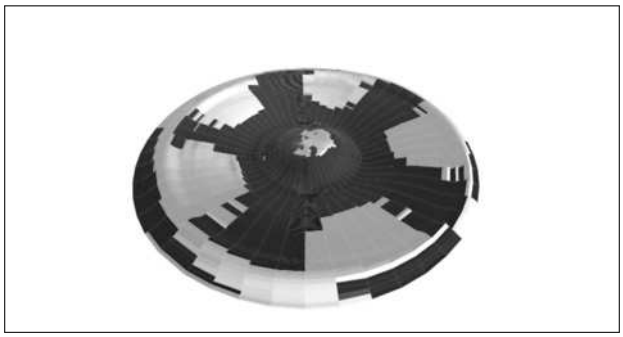

Figure 5.9: Phase pattern of the out-of-phase vibration component at 580 Hz.

The circular modes may be initiated by a non-even mass distribution on the cone. They do not have much influence on the sound radiation because the parts of the cone moving in opposite phase are so close together that their effect cancels out in the total volume velocity at those frequencies. Although the circular modes are not important for the sound radiation, the first circular mode of the surround can cause a significant rocking mode and a rubbing of the coil in the gap.

Ring Resonance

At higher frequencies the vibration of the outer edge of the cone becomes higher and the vibration of the center smaller. Figure 5.10 shows the amplitude of the total vibration at 796 Hz. The total volume velocity generated by the cone and surround

is approximately the same as in the piston mode and the sound pressure level at 1m distance does not change significantly.

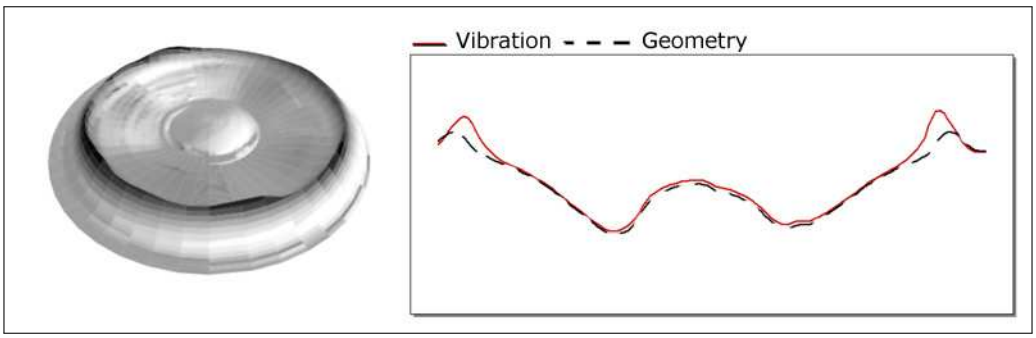

Figure 5.10: Amplitude of the total vibration at 796 Hz.

The application of the sound pressure related decomposition technique, introduced in section 4.1.4, reveals interesting details about the character of the vibration. In figure 5.11 the modeled sound pressure level of the respective vibration components is shown.

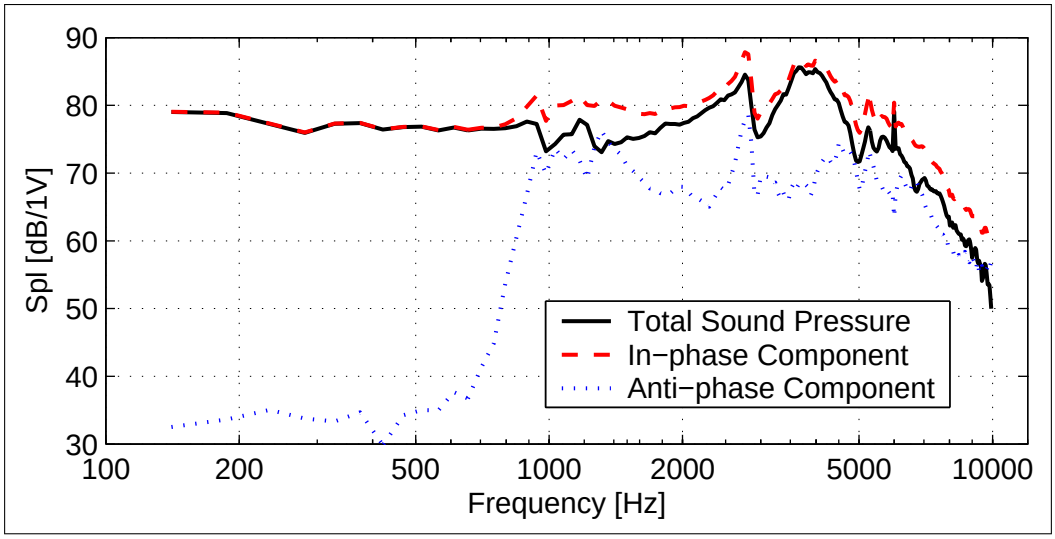

Figure 5.11: Predicted sound pressure at 1 m in axis compared with the sound pressure generated by the in-phase and anti-phase component.

The radiation of the in-phase component minus the anti-phase component results in the total sound pressure level. The third component is out-of-phase in relation to the sound pressure at the model point and therefore it does not contribute anything to the total sound level. Up to a frequency of about 700Hz there is almost no vibration in anti-phase.

Surround Resonance

At a slightly higher frequency (984 Hz) the surround starts vibrating in anti-phase to the ring zone at the outer edge of the cone, see figure 5.12 a). If the volume velocity radiated by the surround (depending on the size of the surround and the displacement) equals the volume velocity radiated by the ring zone of the cone this resonance will not radiate much sound in total. This can be verified by separating the vibration components according to their contribution to the sound pressure at the measurement point.

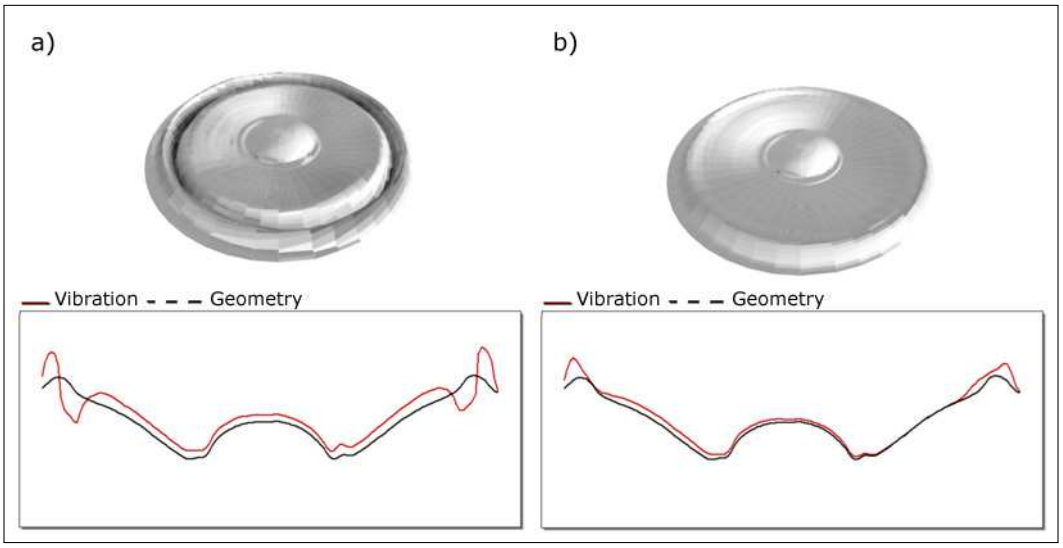

Figure 5.12: a) Amplitude of the total vibration at the surround resonance 984 Hz, b) Amplitude of the in-phase vibration component at the surround resonance.

The in-phase vibration component as shown in figure 5.12 b) shows a piston-like vibration of the inner cone part. The amplitude is relatively small but all points contribute equally to the radiated sound pressure. Figure 5.11 shows that this component produces a sound pressure level which equals the value found at low frequencies. The bending mode of the surround and outer ring zone is almost invisible in the in-phase component.

According to figure 5.11 the anti-phase component alone would generate a sound pressure level which is about 2 dB lower than the level of the total vibration. Thus this component reduces the sound pressure level generated by the in-phase component by 4 dB. The characteristic dip in the frequency response at 984 Hz could be reduced by changing the size of the surround.

Transitional Region

Above the surround resonance more and more bending modes break up starting from the outer side of the cone. At a frequency of 7640 Hz the whole cone is covered by bending modes as shown in the total vibration pattern in figure 5.13 a). But only a small ring at the inner part generates the main contribution of the sound pressure in axis. By looking only at the in-phase vibration component this region can be better identified, see figure 5.13 b).

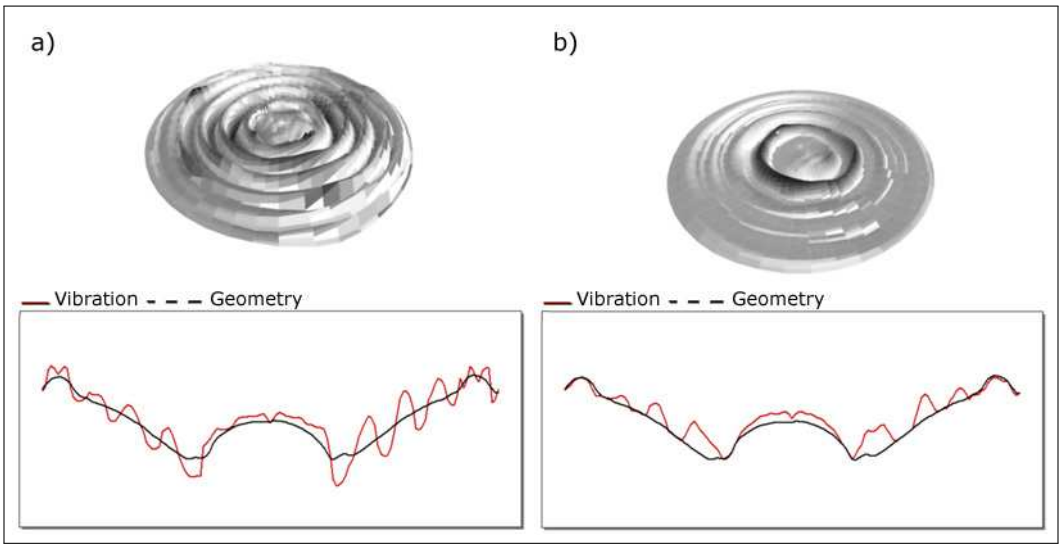

Figure 5.13: a) Amplitude of the total vibration in the 7640 Hz, b) Amplitude of the in-phase vibration component which generates the sound pressure in axis.

Only design changes in the center of the loudspeaker will significantly influence the radiation behavior of the speaker at higher frequencies. The bending motion at the outer areas of the cone do not contribute much to the radiated sound pressure.

6 Conclusion

A proper post-processing is an essential component of vibration measurements on loudspeaker cones. The measurement data has to be prepared for an optimal representation of the vibration properties of the speaker. To obtain an easy interpretable picture of the vibrations an adequate interpolation and error correction method was developed paying attention to the special circumstances applying for the visualization of loudspeaker vibrations.

The immediate link from the cone vibration to the radiated sound pressure is very important for reaching a comprehensive understanding of the loudspeaker behavior. A quick and sufficiently accurate sound pressure modeling method has been implemented and evaluated by comparing the results with real sound pressure measurements. A continuing development of the sound pressure modeling technique is thinkable to further improve the accuracy of the model and to assure its applicability for a higher number of radiation situations. It would be desirable to be able to model the sound pressure of the loudspeaker at arbitrary points also in the near field and for 360° all around the speaker. This is not possible with the implemented point source model but a more sophisticated modeling technique like a boundary element modeling would be necessary. Furthermore it would be an interesting option to be able to predict the loudspeaker radiation for alternative mountings of the speaker not only in an infinite baffle but also in real speaker boxes of arbitrary dimensions.

To provide additional tools for the detailed analysis of the loudspeaker vibrations two novel vibration decomposition techniques were developed. The first decomposition is related to the different vibrational mode shapes on the loudspeaker cone separating them into a component of radial and one of circumferential vibrations. The applicability of this decomposition is given for circular cones provided that the loudspeaker had been properly centered on the turntable during the laser measurement. For oval loudspeakers the single components would be less meaningful because the vibration modes on oval cones are more complicated and can not be separated in such a simple way. However for circular cones a good separation of radial and circumferential vibration modes is possible and provides helpful insight into the mechanical behavior of the cone.

The second developed decomposition technique offers an even greater power to look into the actual problems of the sound radiation. The separation of a vibration component which is in-phase with the total sound pressure at a certain model point reveals the actively contributing vibration areas which are actually responsible for

the radiated sound. Also the two other vibration components created by this kind of decomposition, the anti-phase and the out-of-phase component, contain valuable information about vibration areas which either reduce the total sound pressure or which are irrelevant for the sound pressure at the model point respectively. This information can be used as a starting point to suggest design changes which can effectively counteract problematic peaks and dips in the frequency response of the considered loudspeaker.

The direct conclusion leading to precise suggestions of design changes will however still need more involvement of additional numerical prediction tools. As only the pure vibration data is measured by the laser scanner the visualization software does not have access to the mechanical properties and material data of the cone. But this information would be necessary to precisely predict the effect of e.g. certain changes in geometrical shape, mass distribution, stiffness or damping of selected areas on the cone.

An interesting idea which could improve the prediction of the effects of design changes by only using the vibration data is to totally or partly mask out certain cone areas for the sound pressure modeling. That means the user could decide to remove the influence of a certain area from the sound pressure modeling and then investigate the effect on the total sound pressure for all frequencies. In this way the impact of adding more vibration damping on these selected areas can be predicted provided that the mass and stiffness distribution on the cone does not change substantially. Additional damping will not change the frequencies of the involved modes but only broaden their impact over a wider frequency range while reducing their amplitude. On the other hand changing the mass and stiffness distribution on the cone will shift the frequencies of all involved modes which can totally alter the vibrational behavior of the cone. This is certainly not predictable by the visualization software and needs the involvement of numerical finite element modeling techniques.

An additional visualization of the actual displacement transfer functions at the measurement points would also be an interesting option because it would support the analysis of the mechanical behavior of the cone. That feature will most probably be included in a future version of the visualization software.

To sum up the visualization software developed in this work offers various powerful tools to visualize and analyze the vibration data acquired with the laser scanner. The implemented techniques like interpolation, error correction and sound pressure prediction help to create a comprehensive and easily understandable picture of the measured vibration behavior. An extensively customizable 3D animation and a respective 2D cross-cut animation visualize the vibrational motion of the cone at different frequencies. The actual sound radiation of these vibrations can be analyzed at the same time looking at the frequency response and directivity plots. The implemented data export capabilities allow any easy cooperation of the visual-

ization software together with other applications for presentation of the results or further processing.

The development of the laser scanner hardware and software will continue at Klippel GmbH with the aim to get to a reliable vibration measurement system with unique benefit for loudspeaker manufacturers. The laser scanner software and the visualization software have recently been integrated into one application without any complications and a prototype of the scanning system will be presented at the 121st Audio Engineering Society (AES) Convention in San Francisco in the beginning of October 2006.

References

[Aut 98] Autodesk: *DXF Reference*, Autodesk Inc., Version u14.1.04, June 1998.

[Ber 54] Beranek, Leo L.: *Acoustics*, McGraw-Hill Book Company Inc., New York, 1954.

[BK 82] Brüel & Kjær Primer: *Measuring Vibration*, Brüel & Kjær, Denmark, September 1982.

[Col 99] Colloms, M.: *High Performance Loudspeakers*, John Wiley & Sons, Fifth Edition, Colloms Electroacoustics, UK, 1999.

[Fra 75] Frankort, F. J. M.: *Vibration and Sound Radiation of Loudspeaker Cones*, Ph.D. Thesis, Delft University of Technology, The Netherlands, April 1975.

[Gås 02] Gåsvik, Kjell J.: *Optical Metrology*, John Wiley & Sons, Third Edition, Spectra Vision AS Trondheim, Norway, 2002.

[Her 03] Herrin, D. W., Martinus, F., Wu, T. W. and Seybert, A. F.: A New Look at the High Frequency Boundary Element and Rayleigh Integral Approximations, Technical Paper 01-1451, SAE 2003 Noise & Vibration Conference, Traverse City, USA, 2003.

[Hof 06] Hoffmann, G.: Gaussian Filters, Department of Mechanical Engineering, University of Applied Sciences Emden, Germany, April 2006.

[ISO223] ISO223:2003 *Acoustics – Normal equal-loudness-level contours*, International Organization for Standardization (ISO), 2nd edition, Geneva, 2003.

[Key 05] Keyence: *LK-G Series Product Catalog*, Keyence Corporation, Osaka, Japan, 2005.

[Kli 03] Klippel: *Distortion Analyzer 2 Specification*, Klippel GmbH, Dresden, Germany, November 2003.

[Koh 98] Koch, A. W., Ruprecht, M. W., Toedter, O. and Häusler, G.: *Optische Meßtechnik an technischen Oberflächen*, expert verlag, Germany, 1998.

[Joh 05] Johansmann, M., Siegmund, G. and Pineda M.: *Targeting the Limits of Laser Doppler Vibrometry*, Polytec GmbH, Technical Paper, IDEMA Japan, 2005.

[Mat 04] The MathWorks: *MATLAB® 7 Data Sheet*, The MathWorks Inc., Natick, Massachusetts , 2004.

[Poh 06] Pohl, M.: 3D-Schwingungsmessung an Lautsprechermembranen, Praktikumsbericht, Klippel GmbH, HTW Dresden, Germany, 2006.

[Pol 03] Polytec: *LM Info Special 1/2003*, Polytec GmbH Waldbronn, Germany, 2003.

[Pol 06] Polytec: *Software Manual, Polytec Scan Viewer Version 1.1*, Polytec GmbH Waldbronn, Germany, 2006.

[Zwi 99] Zwicker, E. and Fastl, H.: *Psychoacoustics*, Springer Verlag, Second Updated Edition, Munich, Germany, January 1999.